A $2\frac{1}{2}$ dimensional Thermohaline Circulation Model with Boundary Mixing

by

Hua Ru

B.Sc., Wu Han University (1992)
M.Sc., University of Houston (1997)

Submitted in partial fulfillment of the requirements for the degree of
Master of Science
at the
MASSACHUSETTS INSTITUTE OF TECHNOLOGY
and the
WOODS HOLE OCEANOGRAPHIC INSTITUTION
April 2000

Signature of Author .....
Joint Program in Physical Oceanography
Massachusetts Institute of Technology
Woods Hole Oceanographic Institution
April 26, 2000

Certified by .....
Jochem Marotzke
Associate Professor of Physical Oceanography
Thesis Supervisor

Accepted by .....
Brechner Owens
Chairman, Joint Committee for Physical Oceanography
Massachusetts Institute of Technology
Woods Hole Oceanographic Institution

A $2\frac{1}{2}$ dimensional Thermohaline Circulation Model with Boundary Mixing

by

Hua Ru

Submitted in partial fulfillment of the requirements for the degree of
Master of Science at the Massachusetts Institute of Technology
and the Woods Hole Oceanographic Institution in April 2000

Abstract

A simple quasi-two dimensional dynamical model of Thermohaline circulation (THC) is developed, assuming that the mixing only occurs near western and eastern boundary layers. When the surface density is prescribed, the climatically important quantities, such as the strength of overturning and meridional heat transport, are related to the zonal integral over the vigorously mixing regions and scaled as $(K_v \Delta x)^{2/3}$. The numerical results suggest that the density difference between eastern and western boundaries play an important role in the meridional overturning. The eastern boundary is characterized by the upwelling on top of downwelling. The western boundary layer is featured by the universal upwelling. The inefficiency of diffusion heat transport accounts for the narrowness of sinking region and shallowness of overturning cell in one-hemisphere. The experiments with other surface boundary conditions are also explored. The circulation patterns obtained are similar under various surface temperature distributions, suggesting these are very robust features of THC.

The role of boundary mixing is further explored in global ocean. The $2\frac{1}{2}$ dynamical model is extended to two-hemisphere ocean. Additional dynamics such as Rayleigh friction and abyssal water properties are taken into account. A set of complicated governing equations are derived and numerically solved to obtain steady state solution. The basic circulation features are revealed in our dynamical model. An equtorially asymmetric meridional circulation is observed due to small perturbation at the surface temperature in the high latitude. The density differences between eastern and western boundaries are distinct in both hemispheres. This is achieved during the spin-up process.

Although the dynamical model results agree well with OGCM results in one-hemisphere, several important dynamics are lacking and exposed in two-hemisphere experiments. We need to consider horizontal advection terms which will effectively advect positive density anomalies across the equator and form the deep water for the entire system.

Thesis Supervisor: Jochem Marotzke
Title: Associate Professor of Physical Oceanography

Acknowledgments

My thesis is dedicated to my grandmother, who did not live long enough to read it and come to my commencement. Her deep love for me has been the inspiration accompanying me on my Ph.D. journey.

I would like to take this opportunity to thank Prof. Carl Wunsch, not only because I learned a great deal from his lectures, his papers, his books, but also from my personal interaction with him. He encouraged me at an early stage to pursue this line of research, for which I am grateful. He also carefully read the research paper that was a draft of my thesis.

I would also like to thank my advisor, Prof. Jochem Marotzke. He suggested the thesis topic and guided me through many difficulties. His patience is greatly appreciated. He taught me how to be a responsible scientist.

I am deeply indebted to Jeff Scott for reading my drafts so many times and for his constructive criticism. His comments greatly improved my work. After Prof. Marotzke moved to England, I worked closely with Jeff and consulted with him frequently. It is always a pleasure to discuss questions with him.

Many faculty members at MIT and WHOI helped me in many ways. Among them, Dr. Ruixin Huang and Dr. Mike Spall should be specially mentioned. They both helped me tremendously while I was writing my thesis proposal. Dr. Spall read a draft of my thesis proposal and made very useful comments. Dr. Huang suggested several very interesting projects.

My thanks go to the Joint Committee for Physical Oceanography for their help with my personal difficulties. I am grateful to them for allowing me to transfer to the Joint Program at the end of my second year at MIT. Dr. Breck Owens was always there to listen to me and help me out. Without his help, this thesis would not have been possible. I benefited very much from his constructive criticism which were kindly expressed.

Many students at WHOI and MIT became close friends, including my two office mates Avon Russell and Jason Goodman, Jeff Scott, Constantine Giannitsis, Tieh Yong Koh, Linqing Wen, Tairan Wang, and Yi Zhang. They made my life at MIT colorful and more enjoyable.

I can never give enough credit to my husband, Guohao Dai, for his love, his support, his understanding. He infuses meaning and joy into my life. My sky has been clear blue from the first day I met him.

Contents

Chapter 1

Introduction

1.1 Motivation

The meridional overturning circulation (MOC) plays an important role in poleward heat transport in the ocean and thus is of primary interest to climate models. The present-day MOC is characterized by deep water formation in the North Atlantic ocean and upwelling on a broad scale over much of the Indian and the Pacific ocean (Gordon 1986; Macdonald and Wunsch 1996). The Thermohaline circulation (THC) is driven by the ocean's ability to diffuse heat down to warm the upwelling deep water. In a stratified ocean, turbulent mixing requires mechanical energy. This energy is thought to come from the winds or tides (Munk and Wunsch 1998, hereafter MW98), and probably geothermal sources (Huang 1999). Meanwhile, the oceanic thermohaline circulation is maintained by the water density variation or buoyancy flux. Thus two very important questions are faced and are not clearly understood. One is which of the opposing latitude temperature or salinity constraints dominate the density difference. There are three possible candidates for this problem. The density difference between

the equator and the pole, the one between North and South Atlantic, and the density difference between North Atlantic (NA) and North Pacific (NP). The other question is where the mixing occurs in the ocean and what are the consequences.

The investigation of the first question goes back to Stommel (1961). Stommel's one hemisphere box model provides the qualitative explanation of the multiple steady states in a single hemisphere (e.g. the North Atlantic. Fig.1.1(a)), but our understanding of the THC in the global framework is more complete when a double-hemisphere single-basin box model is considered. Rooth (1982) first proposed the notion that the pole-to-pole density difference in the entire Atlantic might be more important for THC strength. This box model with deep-connected two polar boxes and one equatorial box is further developed by Scott et al. (1999, Fig 1.1(b)). The authors adopted Rooth's box model and showed that if Rooth's picture is true, the equilibrium flow strength q (Fig 1.1.(b)) depends on the pole-to-pole density difference and the fresh water forcing in the upwelling hemisphere only.

Recently, numerous studies in the ocean general circulation model (OGCM) suggested that the THC strength in the North Atlantic in a two-hemisphere single basin system is governed by the pole-to-pole overturning dynamics (Hughes and Weaver 1994; Rahmstorf 1996). Hughes and Weaver (1994) used OGCM and found a linear relation between overturning strength and the difference in vertically integrated steric height (a measure of depth-integrated pressure). Klinger and Marotzke (1999) further justified Hughes and Weaver's result in a temperature-only OGCM. They found that small pole-to-pole temperature differences could set up a markedly asymmetric THC and therefore manifest the amplification of small density asymmetries into large overturning asymmetries. These pictures are in contrast with Stommel's model, where the North Atlantic overturning is a function of the equator-to-pole density gradient.

The second question is related to the mixing in the ocean. The strength of the

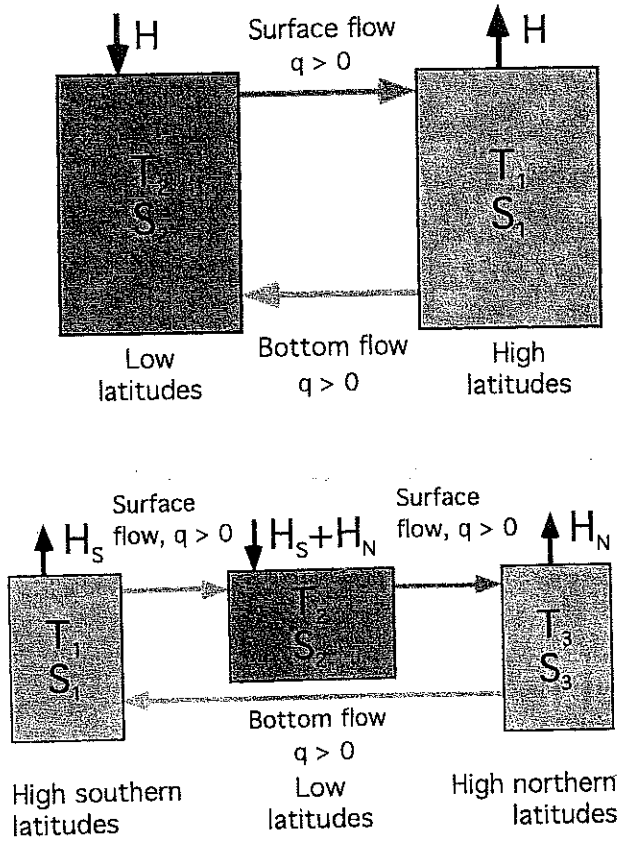

Figure 1.1: (a) Stommel's conceptual model of the THC (Stommel 1961). (b) Rooth's interhemispheric conceptual model of the THC (Rooth 1982). Pictures are adapted from Marotzke 1999.

general circulation of the ocean is closely bound up with the rate at which ocean is mixed (Munk 1966; Munk and Wunsch 1998, hereafter MW98). This is also confirmed in ocean model studies (Bryan 1987; Colin de Verdiere 1988; Zhang et al. 1999). Mixing strength in the ocean might differ between the hemispheres and basins because of variations in roughness of bottom topography (Polzin et al. 1997) or in the energy available for mixing (MW 998; Wunsch 1998). Mixing in the ocean is known not to be uniform but concentrated near the margins (Munk 1966; Wunsch 1970; Armi 1978; Ledwell and Brotkovich 1995; Polzin et al. 1997; MW 98). Marotzke (1997, hereafter M97) investigated the boundary mixing in one-hemisphere single sector ocean and showed that zonally integrated properties did not differ much with the case with uniform mixing. Scott and Marotzke (1999) found that to the lowest order, only the latitudinal position of the mixing matters in the climate importance; the mixing in the low latitudes is important where the ocean is more efficient to transfer heat down to the thermocline. The primary focus of my thesis is to develop a very simple ocean model based on the notion of intense boundary mixing therefore help to understand better the role of boundary mixing in OGCM.

The strength of the general circulation of the ocean is closely bound up with the rate at which ocean is mixed (MW98). The discrepancy between diapycnal mixing rates inferred from large scale budgets (Munk 1966, Hogg 1987) and those inferred from turbulent micro-structure measurement (Gregg 1987) and tracer injection experiments (Ledwell et al 1993) is an intriguing and important paradox in large-scale physical oceanography. A typical mixing rate, which can be approximately represented by vertical eddy diffusivity of density K_v, is of order $10^{-4}m^2s^{-1}$ indicated from large-scale budget; however, 'direct' measurement indicates values of order $10^{-5}m^2s^{-1}$. One possible solution for this paradox is that much of mixing inferred from large-scale budgets occurs in spatially localized regions, such as along boundaries or near rough topography. Examples of enhanced boundary mixing in isolated basins were

presented by Ledwell and Hickey (1995) and Ledwell and Bratkovich (1995). Recent observational evidence for intensified mixing near rough topography in the deep ocean is also consistent with this idea (Polzin et al 1997).

The recent works of Marotzke(1997, hereafter M97) and Samelson(1998) have both explored boundary mixing case numerically. The former analyzed a 3-D GCM with non-zero vertical mixing coefficient K_v only near both side boundaries and in convection regions, while the latter focused on localized enhanced vertical diffusivity near the eastern boundary layer. The scaling dependence on diapycnal mixing is very similar in both papers. They are consistent with previous studies that the strength of the meridional overturning cell (MOC) is strongly dependent on the value of the vertical (or diapycnal) eddy diffusivity K_v (Bryan 1987; Winton 1996; Colin De Verdiere 1988), which is the mechanism that provides the necessary warming of the rising abyssal water.

The overarching goal of my thesis is to understand how the east-west density differences maintain meridional overturning in thermal-wind balance. This thesis will touch two aforementioned questions. What controls the North Atlantic overturning ? Where are the consequences if the enhanced mixing occurs near lateral boundaries? We developed a simple dynamical numerical model which depends primarily on thermal wind balance and other thermodynamic considerations. The model results in expressions for the zonal-mean zonal density gradient (more specifically, eastern and western boundary density), as a function of latitude and depth, and the meridional overturning in a one-hemisphere single basin ocean, and then extend this model to the strength of cross-equatorial transport in a two-hemisphere single basin ocean system. We will mainly focus on the rotating fluid dynamics of the global THC.

The starting point is M97. Our simple boundary layer model is an extension of previous work of M97. It was motivated by the fact that even when the mixing is

uniform, the vertical motion is very closely confined to east and west lateral boundaries; by the striking similar scaling law for both uniform and boundary mixing (See Park and Bryan 2000, they gave very good review of previous scaling analysis); and by the recent microstructure observations. As such that the boundary mixing represent a very important and basic dynamics of the thermohaline circulation (THC). The 3-D GCM runs with boundary mixing showed much cleaner scaling behavior, leading to considerable theoretical simplification, but the gross, integrated properties didn't differ much from the case with uniform mixing. This means, in particular, that the boundary-mixing theory developed here is likely to carry over to the case with uniform mixing.

The quasi two-dimensional (y,z) model used in this study is described in chapter 2. This model includes the basic ingredients of all the THC models: Dynamics on the rotating earth; The meridional mass transport in thermal wind balance, which is achieved by modeling not the zonally averaged density directly, but rather splitting the tracers up in eastern and western boundary field (hence a $2\frac{1}{2}$ dimensional model). The result is a model that is economical to run, so that a large number of experiments can be performed. In this study, we will focus on understanding the role of boundary mixing in determining integral properties of the THC, the scaling behavior and the dynamics of the boundary mixing, therefore providing a self-consistent and theoretical foundation for M97 and Marotzke and Klinger (2000). It is not intended to produce the exact results of OGCM. Rather, it is intended to mimic the results of M97 and help us understand the complex model behavior of 3-D GCM results efficiently. For examples: What will the ocean circulation look like if we assume the ocean mixing occurs in spatially localized region? Can we obtain a self-consistent dynamical description of THC under boundary mixing, assuming that all relevant processes occur in the side-boundary layers? What is the scaling law that best relates the vertical diffusivity to climatically important quantities, like meridional overturn-

ing cell (MOC) and poleward heat transport? In particularly clear way, the model illustrates a number of most important dynamics in controlling the ocean circulation.

It is important to mention that the mechanism of heat transport by the ocean is very different from that by the atmosphere. Ocean heat transport is in many ways determined by the presence of lateral boundaries (Colin De Verdiere 1988). Were it not for their presence, the ocean could react to differential heating by setting up a zonal circulation in thermal wind balance. Baroclinically unstable eddies could then play the role of heat transport if the meridional temperature proved unstable to perturbation, in a process similar to what takes place in the atmosphere. With continental barriers such zonal circulations are forbidden in the ocean. It is the purpose of this thesis to illustrate the link of the strength of ocean circulation and thus heat transport with the density difference at two lateral boundaries, i.e. eastern and western density difference.

The thesis is organized in 5 parts. The model designed in this study is described in chapter 2. The main numerical results are illustrated. The scaling analysis and interpretation are given in chapter 2 as well. In chapter 3, other numerical experiments with different boundary conditions are carried out. In chapter 4, the model is further developed to explore the effects of boundary mixing in the global THC, which is a 1-basin system in double-hemisphere. We focus on understanding the dymanics. Discussion and summary of the model are presented in Chapter 5.

Chapter 2

A simple $2\frac{1}{2}$ dimensional dynamical model in 1-hemisphere, 1-basin system

2.1 Formulation of the model: the assumptions and governing equations

Following previous work of Marotzke (1997), we now postulate a quasi-two dimensional(y,z) boundary layer model of THC. We assume that the vertical advections are totally confined to the western and eastern boundary layers, as is the vertical mixing. The thickness of western boundary layer Δx can be estimated as the maximum thickness of Munk layer, Stommel layer or inertial layer, which depends on different vorticity balances within the western boundary current. As the width of the eastern boundary, we simply assume it is equal to the western boundary. The motion in the interior which connects the two boundary layers is entirely zonal. The model can

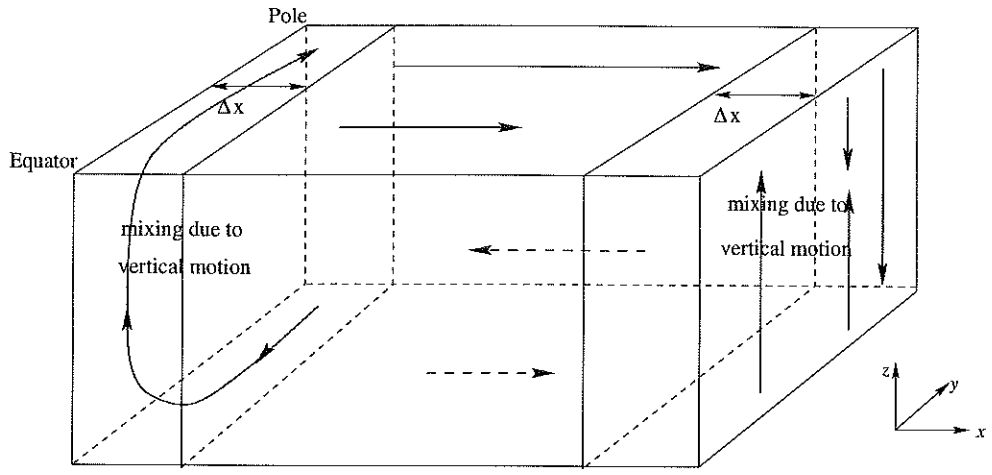

Figure 2.1: Schematic ocean circulation model on boundary mixing

be sketched schematically as in Fig 2.1. Based on the assumption that the mixing only occurs near the boundaries, and there is no wind stress on the surface or bottom topography, we can write down the following equations. Notation is standard; subscripts E and W stand for eastern and western boundary, respectively. All variables are functions of latitude and depth except where explicitly indicated.

i) Surface density is given and is a function of latitude only; the abyss uniformly has the properties of the densest surface water.

$$\rho_W(y,0) = \rho_E(y,0) = \rho_s(y) = \rho_P + (\rho_T - \rho_P)(1 - y/L_y) \tag{2.1}$$

$$\rho_E(y,-H) = \rho_W(y,-H) = \rho_P \tag{2.2}$$

where y is latitude, L_y is meridional extent, and ρ_T and ρ_P are surface densities at the southern('tropical') and northern('polar') walls, respectively.

ii) Density in the grid cells at the lateral boundary is governed by vertical advective-diffusive balance. The model equations are supplemented by a convective adjustment scheme to prevent the development of static instabilities. It turns out for the fixed surface density, such as *i*), this adjustment scheme is not necessary. This

point will be taken up later in the paper. There is no vertical mixing in the interior.

$$W_W \frac{\partial \rho_W}{\partial z} = K_v \frac{\partial^2 \rho_W}{\partial z^2} \tag{2.3}$$

$$W_E \frac{\partial \rho_E}{\partial z} = K_v \frac{\partial^2 \rho_E}{\partial z^2} \tag{2.4}$$

iii) Along the equator, isopycnals are level since there is no wind stress to balance zonal pressure and density gradients. The density of the western and eastern boundary must meet at the equator.

$$\rho_E(0, z) = \rho_W(0, z) \tag{2.5}$$

iv) Isopycnals are flat in the zonal direction except in the western boundary current. The interior density approximately equals to eastern boundary density (M97, Fig(5)). Through Rossby wave activity, density in the interior is assumed largely to follow that of the eastern boundary, right until the western boundary current.

v) Thermal wind relation

$$\frac{\partial V_W}{\partial z} = -\frac{g}{\beta y \rho_0} \frac{\rho_E - \rho_W}{\Delta x} \tag{2.6}$$

$$\frac{\partial V_E}{\partial z} = 0 \tag{2.7}$$

and

$$\frac{\partial U}{\partial z} = \frac{g}{\beta y \rho_0} \frac{\partial \rho_E}{\partial y} \tag{2.8}$$

Again Δx is the width of both lateral boundary layers. It is assumed that the vigorous meridional velocity mainly occurs at the western boundary. The meridional velocity at the eastern boundary is weak and close to zero. This assumption is rooted in and

justified from the observation of OGCM results when the surface wind is turned off. In the real ocean, there is a meridional current near eastern boundary mainly due to the existence of surface wind. Notice that the equatorial β-plane approximation has been made, and it is assumed, following *iv*), that the zonal flow, U, is constant and in balance with the zonal mean meridional density gradient, which in turn is identical to the eastern boundary density gradient.

vi) Mass conservation, as applied to the eastern and western boundary layers:

$$\frac{\partial W_W}{\partial z} = -\frac{\partial V_W}{\partial y} - \frac{U}{\Delta x} \tag{2.9}$$

$$\frac{\partial W_E}{\partial z} = \frac{U}{\Delta x} \tag{2.10}$$

At the eastern boundary, $\frac{\partial U}{\partial x} \rightarrow -\frac{U}{\Delta x}$; While at the western boundary, $\frac{\partial U}{\partial x} \rightarrow \frac{U}{\Delta x}$.

vii) In the absence of wind, bottom topography, and momentum advection, the vertically averaged velocity is zero everywhere, which automatically fulfills the rigid-lid and solid-bottom boundary conditions, and which obviates the need to find a level of no motion.

From eqn (2.10), taking the derivative with depth z and combining with eqn (2.8), we get

$$\frac{\partial U}{\partial z} = \Delta x \frac{\partial^2 W_E}{\partial z^2} = \frac{g}{\beta y \rho_0} \frac{\partial \rho_E}{\partial y} \tag{2.11}$$

or

$$\frac{\partial^2 W_E}{\partial z^2} = \frac{g}{\beta y \rho_0 \Delta x} \frac{\partial \rho_E}{\partial y} \tag{2.12}$$

From eqn (2.9), taking the derivative with depth z, we obtain

$$\frac{\partial^2 W_W}{\partial z^2} = -\frac{\partial^2 V_W}{\partial y \partial z} - \frac{1}{\Delta x}\frac{\partial U}{\partial z} \tag{2.13}$$

From eqn (2.6), taking the derivative with y,

$$\frac{\partial^2 V_W}{\partial y \partial z} = \frac{g}{\beta y \rho_0 y^2}\left(\frac{\rho_E - \rho_W}{\Delta x}\right) - \frac{g}{\beta y \rho_0 \Delta x}\frac{\partial\left(\rho_E - \rho_W\right)}{\partial y}$$

Substituting above equation and (2.11) back into (2.13), we have

$$\frac{\partial^2 W_W}{\partial z^2} = -\frac{g}{\beta y \rho_0 \Delta x}\left(\frac{\rho_E - \rho_W}{y} + \frac{\partial \rho_W}{\partial y}\right) \tag{2.15}$$

The following final diagnostic equations which only contain ρ_W, ρ_E, W_W, W_E are derived.

$$\frac{\partial^2 W_W}{\partial z^2} = -\frac{g}{\beta y \rho_0 \Delta x}\left(\frac{\rho_E - \rho_W}{y} + \frac{\partial \rho_W}{\partial y}\right) \tag{2.16}$$

$$\frac{\partial^2 W_E}{\partial z^2} = \frac{g}{\beta y \rho_0 \Delta x}\frac{\partial \rho_E}{\partial y} \tag{2.17}$$

plus the other two prognostic equations from *ii*)

$$\frac{\partial \rho_W}{\partial t} + W_W \frac{\partial \rho_W}{\partial z} = K_v \frac{\partial^2 \rho_W}{\partial z^2} \tag{2.18}$$

$$\frac{\partial \rho_E}{\partial t} + W_E \frac{\partial \rho_E}{\partial z} = K_v \frac{\partial^2 \rho_E}{\partial z^2} \tag{2.19}$$

The dynamical model is numerically solved as an initial value problem using finite difference methods. Given any initial conditions of ρ_W and ρ_E, W_W and W_E are solved from Eqn (2.16) (2.17). Then using Eqn(2.18) (2.19), the next step ρ_W and

ρ_E are derived. Steady-state solutions are obtained by time stepping to equilibrium. The time step is modified CFL since the equations are second-order differential ones, $\Delta t \leq \frac{\Delta z^2}{max(|W_W|,|W_E|)\Delta z + 2K_v}$. We consider the model at steady state if the overturning streamfunction satisfies $|\psi^{t+\Delta t} - \psi^t| < \epsilon(10^{-10})$. After W_W and W_E are solved, we can get V_W and U from continuity equations.

A northern hemisphere basin extends from 1° to 64° north, the bottom of the basin is at a constant depth of 4000m, Δx is chosen as 400km. It is unclear whether Δx will change with larger K_v in more sophisticated model. But for simplicity, we will keep Δx as constant. A linearized equation of state depending only on temperature has been used, with the thermal expansion coefficient $\alpha = 2 \times 10^{-4} {}^\circ C^{-1}$. Therefore, buoyancy and temperature will be used interchangeably in the discussion of the experiments. In section 3, $\rho_T = 1023 kgm^{-3}$, $\rho_p = 1029 kgm^{-3}$, which corresponds to $T_T = 30^\circ C$ and $T_p = 0^\circ C$. The no-normal flow condition was applied at four lateral walls. Thus a meridional overturning streamfunction (ψ) can be defined from zonal no-normal flow requirement. Detailed numerical consideration is listed in appendix.

2.2 Main results

For linear surface forcing, we get extremely good agreement with M97. Fig.2.2 (a)(b) shows a typical case of $K_v = 5 \times 10^{-4} m^2 s^{-1}$.

Near the western wall, there is upwelling only and everywhere. Near the eastern wall, there is a consistent pattern of downwelling above upwelling with downwelling reaching deeper at high latitudes. The different vertical velocity patterns between eastern and western boundaries are reflected in the density sections along the walls.

In the west, the water is stratified everywhere except at the northern boundary,

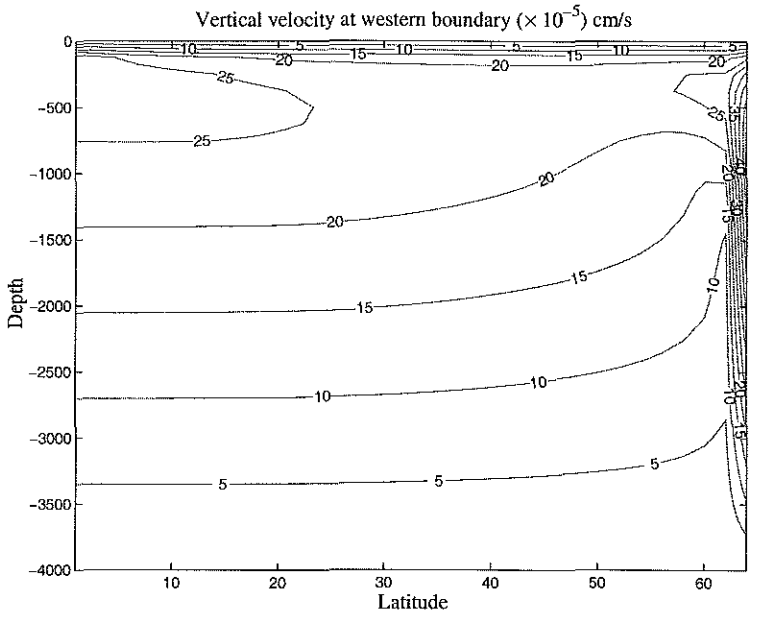

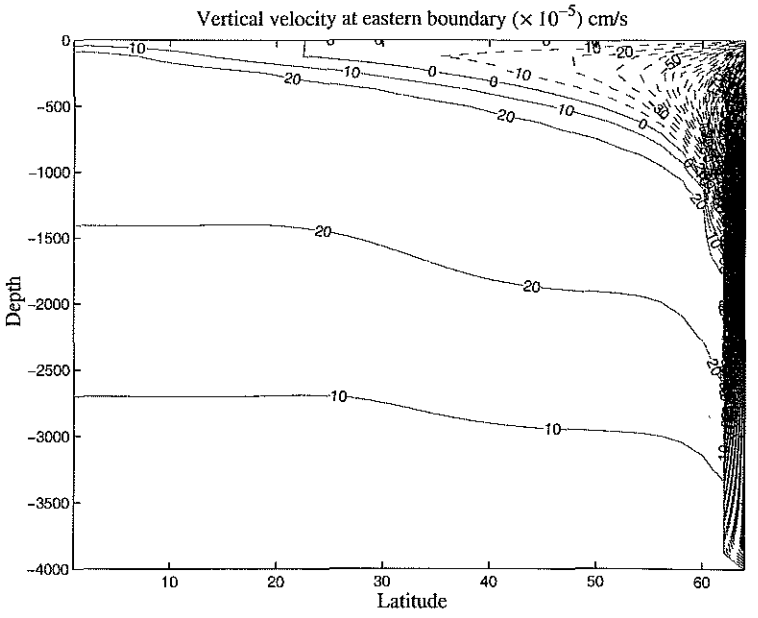

Figure 2.2: (a) Vertical velocity at western boundary, contour interval $5 \times 10^{-5} cms^{-1}$. (b) Vertical velocity at eastern boundary, contour interval $10 \times 10^{-5} cms^{-1}$.

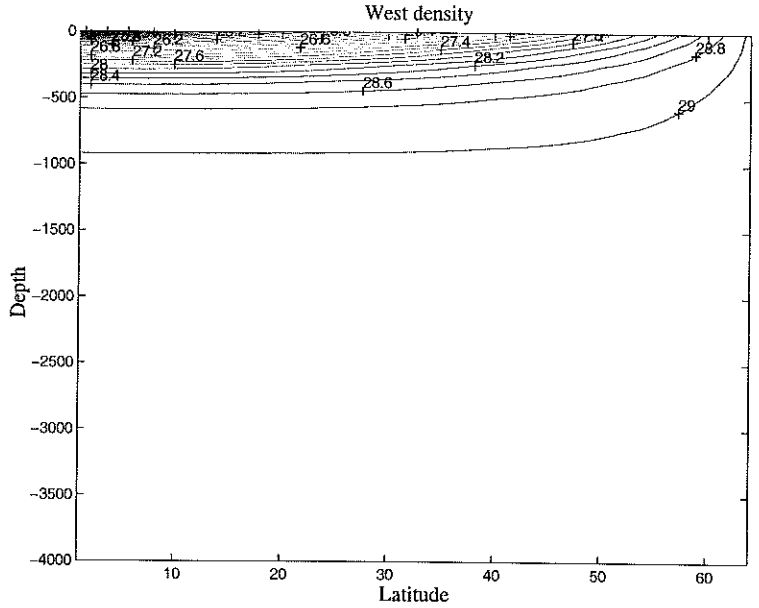

Figure 2.3: Western boundary density. Contour interval is $0.2kgm^{-3}$.

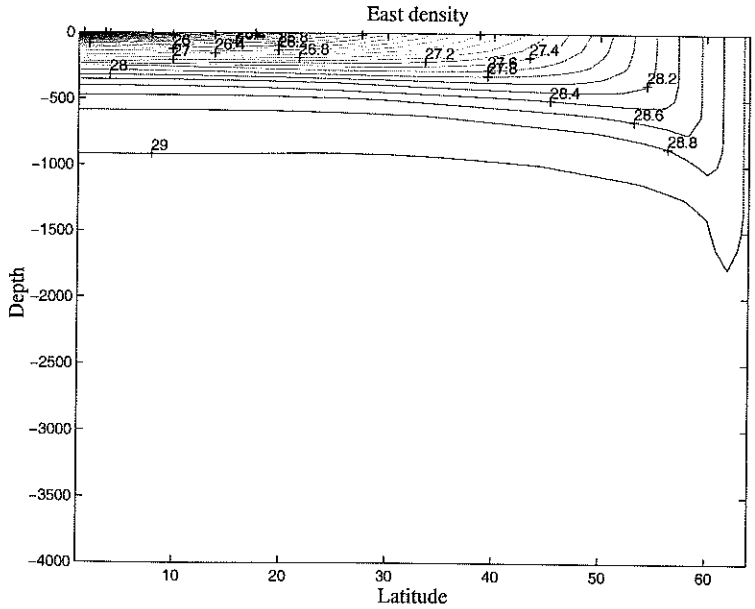

Figure 2.4: Eastern boundary density. Contour interval is $0.2kgm^{-3}$.

and stratification is strongest near surface (Fig 2.3). In the east, the near-surface meridional density gradient implies eastward surface current (Fig 2.4). When this flow impinges on the eastern wall, it sinks and hence downwells in the high latitude. Away from the equator poleward, the meridional density gradient reaches deeper, near surface eastward flow is stronger, therefore the downwelling is stronger with latitude (Fig 2.2(a)(b)). At high latitudes, downwelling (not convection) leads to neutral stratification to a depth that increases with latitude. Between 400m and 1500m, isopycnals slopes downward with latitude. In response to this density structure, a westward shear is established, consistent with the need to provide a pathway for the vertically converging waters (Fig 2.2(b)) (Marotzke 1997). We can see this clearly from Fig 2.5(a). The zonal flow is layered, with westward flow underneath it, eastward flow in the deep ocean (not shown due to contour interval). Meanwhile, the eastward surface flow tends to pile up water near the eastern boundary and thus ensue a northward meridional current at western boundary. It is assumed the meridional velocity at the eastern boundary vanishes. Fig 2.6(a) displays the density difference between eastern and western walls, a measure of vertical shear of meridional velocity. The density difference becomes stronger and extends to greater depths with latitude.

The upwelling over downwelling in the eastern boundary is a very robust feature in the model. First, eastern downwelling homogenizes the water column with surface water to a certain depth Z_ρ. The result will be lower density (warmer temperature) at eastern than that at the western wall. The downwelling changes the density to neutral stratification up to Z_ρ. Below this depth, flow must be continuously downward since stratification (due to diffusion) increases with depth until the maximum stratification is reached where the vertical velocity is zero. There is a transition region beneath the downwelling zone where stratification increases with depth, then reaches maximum and decreases. Consequently, at eastern boundary, the stratification implies

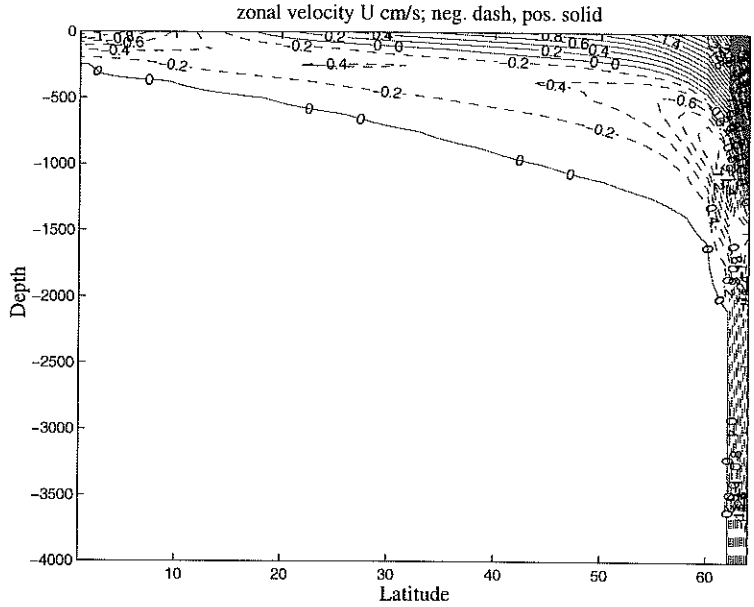

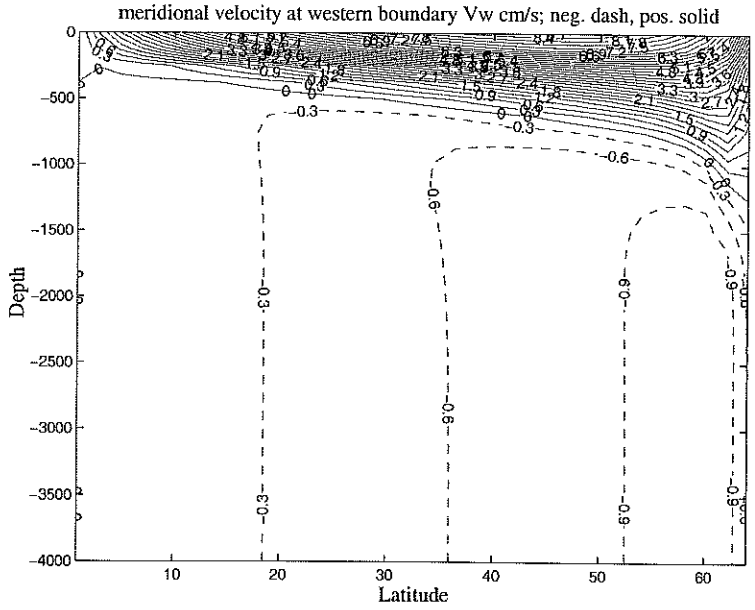

Figure 2.5: Boundary mixing case, $K_v = 5 \times 10^{-4} m^2 s^{-1}$. (a) Zonal velocity, contour interval $0.2 cms^{-1}$. (b) Meridional velocity at western wall, contour interval $0.3 cms^{-1}$. Solid line: positive; dash line: negative value.

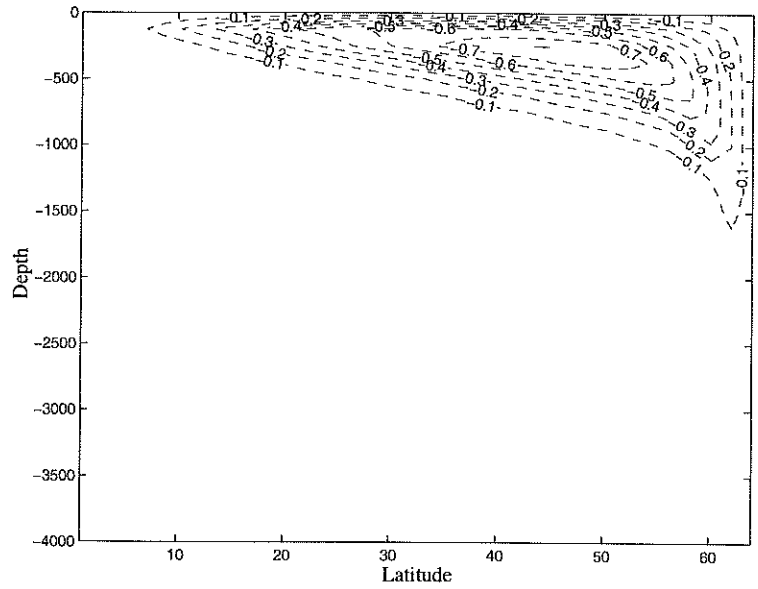

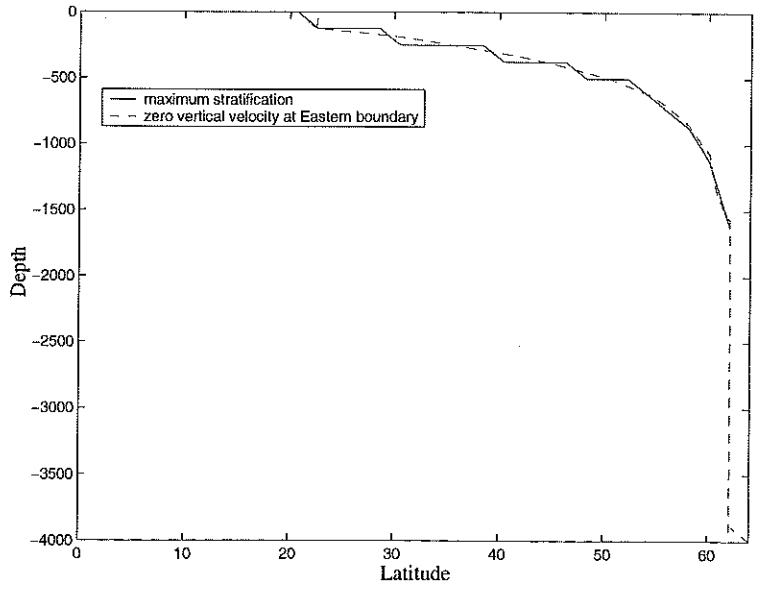

Figure 2.6: (a) Density difference as eastern wall minus western wall, solid line:positive, contour interval $0.005 kgm^{-3}$; dash line: negative value. contour interval $0.1 kgm^{-3}$. (b) Pycnocline and zero vertical velocity near eastern boundary. Solid line: positive; dash line: negative value.

downwelling, and no motion and then upwelling.

It is evident in Fig 2.6(b) that the line of maximum stratification (pycnocline) at the eastern boundary coincides with the line of zero vertical velocity, which separates downwelling and upwelling. The place where the vertical velocity changes sign is where the maximum stratification is reached. Similarly, at western boundary, the maximum stratification is near the surface. Hence ample upwelling is everywhere in the western boundary.

The strong upwelling along the western boundary layer can be explained as follows. Because of the geostrophic approximation applied within the western boundary region, the total amount of mass flux can be estimated by density difference across the boundary, divided by the local Coriolis parameter (Eqn(2.6)). With the β-plane approximation, the Coriolis parameter increases linearly with latitude. As a result, to transport the same amount of mass flux through the western boundary current, the east-west temperature difference at mid-latitude has to be larger than that at lower latitude. Since the water at western wall is colder than that at eastern wall, the larger east-west temperature difference means cold water must upwell within the western boundary layer. This upwelling in turn increases the total amount of mass flux in the western boundary region, which requires an even larger east-west temperature contrast. Therefore, upwelling is an intrinsic mechanism of the western boundary current imposed by the lowest order of dynamics, such as geostrophy and mass conservation (Huang and Yang 1996).

The thermohaline circulation can be visualized by plotting the zonally integrated meridional overturning streamfunction. The meridional overturning strength for $K_v = 5 \times 10^{-4} m^2 s^{-1}$ is about the right order of magnitude, the maximum overturning happens at about 1000 m(Fig 2.7). This implies that when the northward meridional flow reaches the pole, it gets cold and sinks, then returns over a somewhat

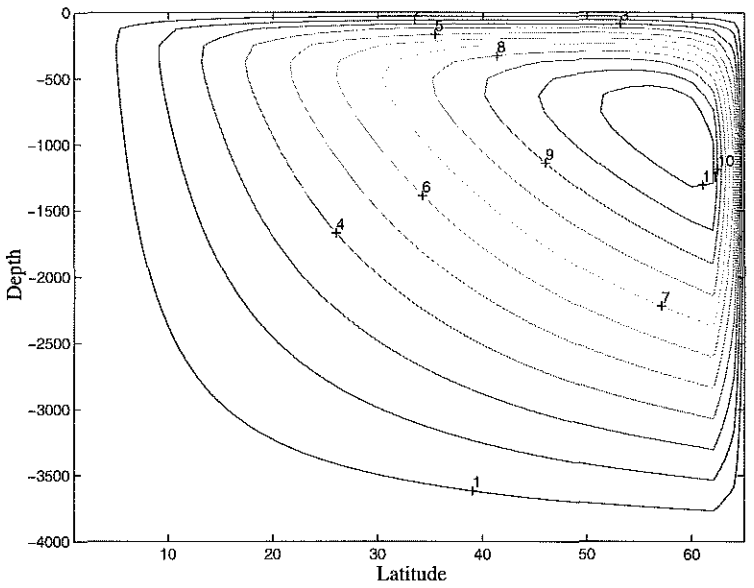

Figure 2.7: Meridional streamfunction, the flow field is clockwise around the center. Contour interval is 1 Sv.

broader depth than in M97 (M97 Fig.7(a)). The maximum overturning streamfunction is very close to poleward boundary. This is comparable to M97, Winton(1997), Park and Bryan(2000). The downwelling branch of the meridional circulation is confined to the region near the northern wall.

We found particularly in this model, the steady state solution can be obtained without convection scheme. There is a strong indication that convection scheme is not an essential element in this numerical part. Contrary to M97, who suggested that convection sets the neutralization depth Z_ρ, we found that the depth Z_ρ is mainly determined by downwelling. As discussed later in Marotzke and Scott(1999), the violent convective mixing and downwelling are two fundamentally different processes. Convection adjustment mixes the whole water column to the bottom, while the downwelling neutralizes the interior density to the surface density to depth Z_ρ. In the model prescribed here, the strongest downwelling to bottom only occurs at northeast corner, within one grid cell from northern wall when $K_v = 5 \times 10^{-4} m^2 s^{-1}$. Because of the deep boundary condition imposed, i.e. the abyssal water has the

property of coldest (polar) surface water property, we actually implicitly employ the consequence of convection procedure. This boundary condition also limited where the downwelling and deep water formation should occur. For the fixed surface boundary condition, strongest downwelling coincides with the location of coldest surface water. Therefore, specifying the temperature of deep water substitutes the role of convective mixing at eastern boundary, and steady state solution can be solved without explicit convection adjustment procedure.

The asymmetry between downward and upward branch of MOC is obvious for small K_v. For different K_v experiments, with K_v ranging from 5 to $500 \times 10^{-4} m^2 s^{-1}$, a similar qualitative picture of vertical motions, meridional and zonal flows is obtained. The south-north asymmetry is less when the downwelling at eastern wall gets wider for bigger diffusivity coefficient. When vertical diffusion gets more efficient, the upwelling near western boundary (W_W) increases. The zonal flow across ocean which is affected by the western upwelling gets stronger. Therefore, at eastern wall, downwelling and vertical isopycnal at the same latitude reach deeper. The region of downwelling gets wider (Fig 2.8). The wider sinking branch folds the considerable surface density gradient between mid-latitude and the pole into vertical, producing substantial vertical density gradients in the deep ocean.

In our experiments, the narrowness of sinking is persistent for small K_v. Clearly this strong asymmetry does not directly own to the existence of rotation, otherwise the asymmetry will appear even for big K_v. In order to understand a complete ocean circulation pattern, we have to answer an important and interesting question: What is the physical cause for the narrowness of deep sinking region? We can quantify the relative importance of downwelling to diffusion by non-dimensional Peclet number $\frac{\psi_{max}}{\Delta x K_v}$ (Marotzke et al 1988, Winton 1995). As shown later in this paper, ψ_{max} has roughly a $\frac{2}{3}$ dependence on K_v over most of the range of experiments. Consequently, the importance of downwelling is decreased with increasing K_v (third column of Table

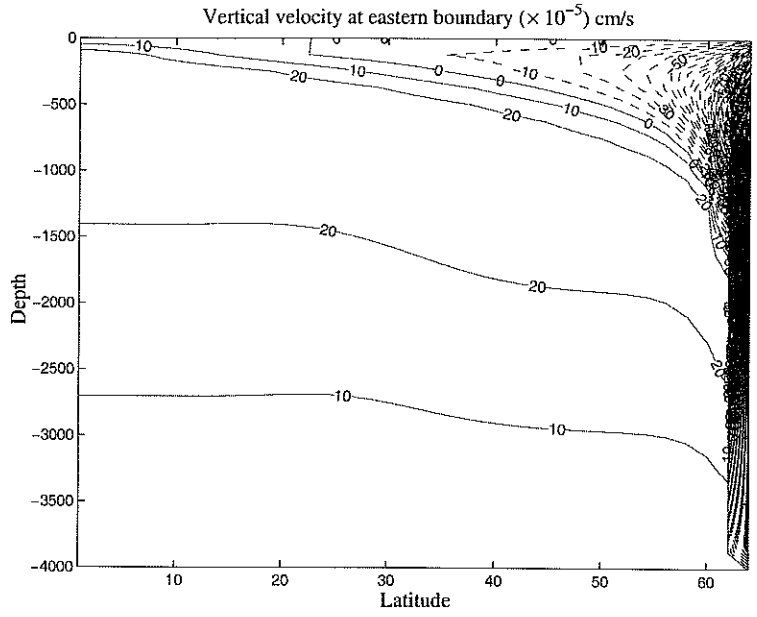

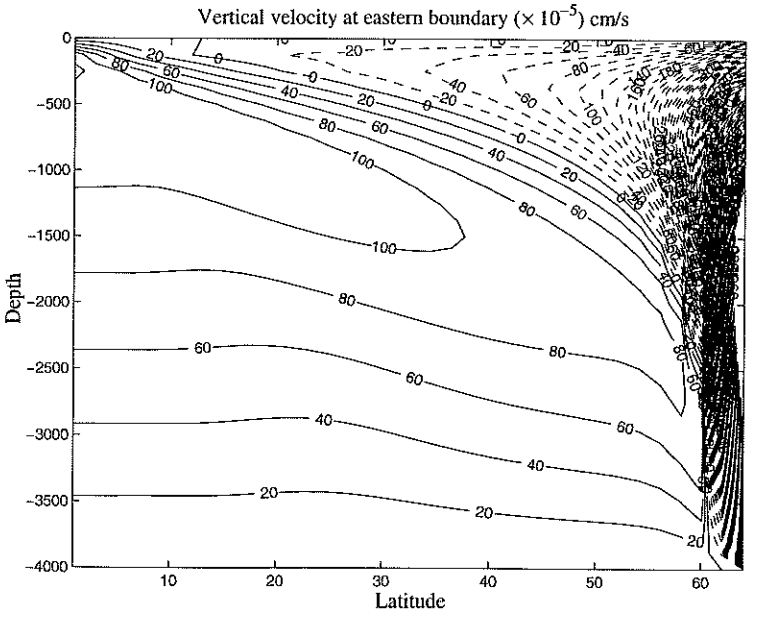

Figure 2.8: vertical velocity at eastern wall for different K_v runs, (a) when $K_v = 5 \times 10^{-4} m^2 s^{-1}$. (b) when $K_v = 39 \times 10^{-4} m^2 s^{-1}$.

1). At steady state, the downward diffusion of heat must balance the cooling by downwelling, which forms the cold deep water. The diffusive heat transport is directly proportional to K_v, whereas the downwelling at eastern boundary is a relatively weaker dependence on K_v (approximately $K_v^{2/3}$). As K_v is increased, the diffusive warming becomes relatively more efficient than the cooling by downwelling. Therefore the narrowness of the downward branch is a measure of inefficiency of diffusive heat transport. In this sense, meridional overturning circulation resulting from mixing process can be thought of as 'pulled up' by the downward diffusion rather than 'pushed down' by downwelling. When K_v becomes bigger, the downward branch gets wider. This is consistent with our observation. During the experiments, the time required to reach steady state decreases with increasing K_v, where the same initial conditions and the same equilibrium criteria were applied. To understand why the sinking is as narrow as it is now, or how small the diffusivity should be in order to get narrow sinking, we have to seek for the oceanic energetics (Winton 1995, Munk and Wunsch 1998).

The argument here for narrowness of sinking is somewhat different from Rossby's. According to Rossby(1965), which stated that the convection cools the water efficiently, it acts as heat sink and is independent of K_v. Because convection is much more efficient, the area of turbulent mixing must be accordingly larger. But in this model, the heat balance is solely between the heating due to diffusion and upwelling of the abyssal cold water, which is supplied by downwelling at northeast corner. Thus downwelling acts as heat sink 'provider'.

Marotzke and Scott(1999) looked at the narrow sinking from another interesting aspect by invoking 3-D dynamical vortex interaction. However, the vortex picture is not applicable here. As we discussed before, it is a robust feature in THC that the downwelling adjacent to upwelling in the eastern boundary layer. The downwelling will cause vortex tube stretching in the upper part and vortex tube compression in

the lower part of the water column, which will cause a positive vorticity tendency in the upper region and negative tendency in the lower region. The upwelling will cause the opposite vorticity tendency. Thus in the deep ocean along eastern wall, there are indeed a clockwise circulation on the downwelling site and anti-clockwise upon upwelling site next to it. These two vortices attract and push toward each other and make the sinking region very narrow (Marotzke and Scott 1999). But it is uncertain the effects of the upper level vortices, which tend to propagate in the opposite direction and make the sinking region wide. Therefore, the model we reported here is much closer to Rossby's 2-D model from point of view narrow sinking.

The explanation above can also help us understand the shallowness of the overturning circulation. When vertical diffusivity is small, the upwelling near the western boundary is weaker. Correspondingly, the eastern downwelling and depth Z_ρ will be shallow. The shallowness of the MOC is governed by mid-latitude downwelling depth Z_ρ, which is eventually influenced by K_v. It is downwelling that determines the depth of the maximum overturning. The flow simply downwells and then returns at much shallower depth than in Stommel-Arons' picture.

As K_v is increased, the circulation intensifies, the center of the cell moves down reflecting the increasing density gradients at the bottom(Fig 2.9). The center of the cell also moves southward with increasing K_v, the northward boundary layer and perhaps the top boundary layer disappeared. When K_v is really big ($K_v = 1,000 \times 10^{-4} m^2 s^{-1}$), the cell almost approaches a symmetric limit circle (Fig 2.9 (10)). If K_v is increased further to 5,000 or 10,000 $\times 10^{-4} m^2 s^{-1}$, MOC continues to move equatorward and establishes a narrow rising branch near the equator, indicating that the diffusion becomes very efficient. It is interesting to note that the movement of streamfunction described is analogous to Rossby(1998). Rossby's numerical experiment is on a non-rotating system, where a square box of water is forced by non-uniform heating from below. When Rayleigh number is large, there is ex-

treme asymmetry of the circulation. The circulation becomes weaker and symmetric at the limit of low Rayleigh number. Whereas in our model, the ocean circulation is relatively weak and strongly asymmetric at small vertical diffusivity. There is a clear tendency for the MOC to continue move equatorward and becomes stronger at large vertical diffusivity. The experiments are summarized in Table 1, which also include the thermocline depth at $30°N$, the maximum of east-west density difference. The latter increases only slightly as K_v is increased (fifth column of Table 1).

Table 1. Summary of experiments with a linear temperature distribution

$K_v(\times 10^{-4} m^2 s^{-1})$	ψ_{max} (Sv)	$\psi_{max}/K_v\Delta x(\times 10^{-3})$	D (m)	$(\rho_E - \rho_W)_{max}(kgm^{-3})$	H_{max} (PW)
5	12	59	209	-0.802	0.27
8	17	50	258	-0.796	0.39
14	23	41	323	-0.823	0.55
23	31	34	400	-0.829	0.78
39	42	27	490	-0.843	1.10
65	57	22	593	-0.862	1.53
108	74	17	704	-0.881	2.11
180	96	13	817	-0.910	2.87
300	119	10	925	-0.949	3.83
500	145	7	1022	-1.000	5.02
1000	173	4	1127	-1.041	6.93
5000	245	1	1252	-0.816	13.1

A power law relationship for maximum of streamfunction is obtained for different K_v ($K_v^{2/3}$) (Fig 2.10(a)).

We can calculate the thermocline thickness at a single point by (Park and Bryan

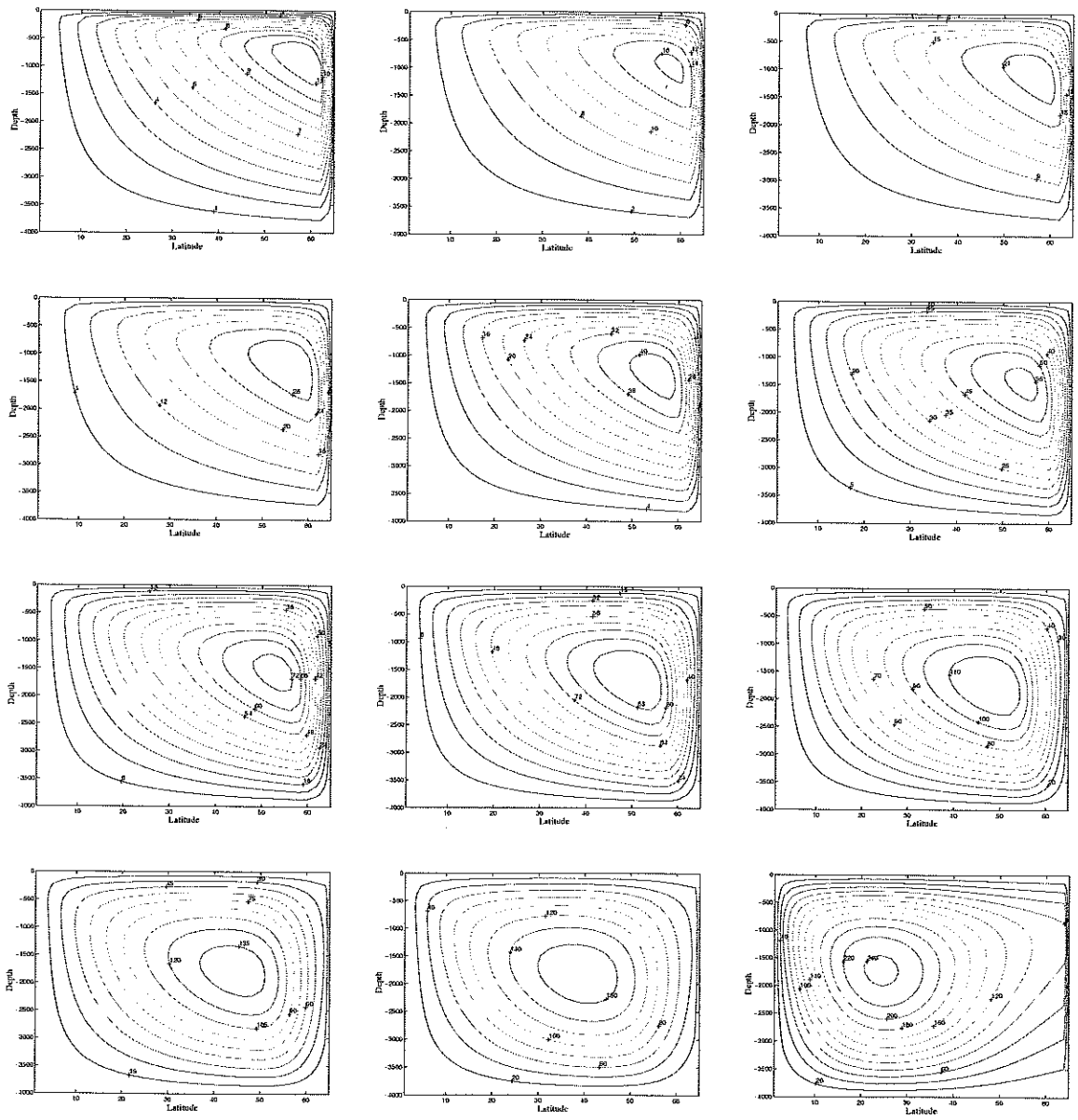

Figure 2.9: $\psi(y,z)$ at different K_v numbers 5, 8, 14, 23, 39, 65, 108, 180, 300, 500, 1000, 5000 $\times 10^{-4} m^2 s^{-1}$. The contour intervals are different at each case.

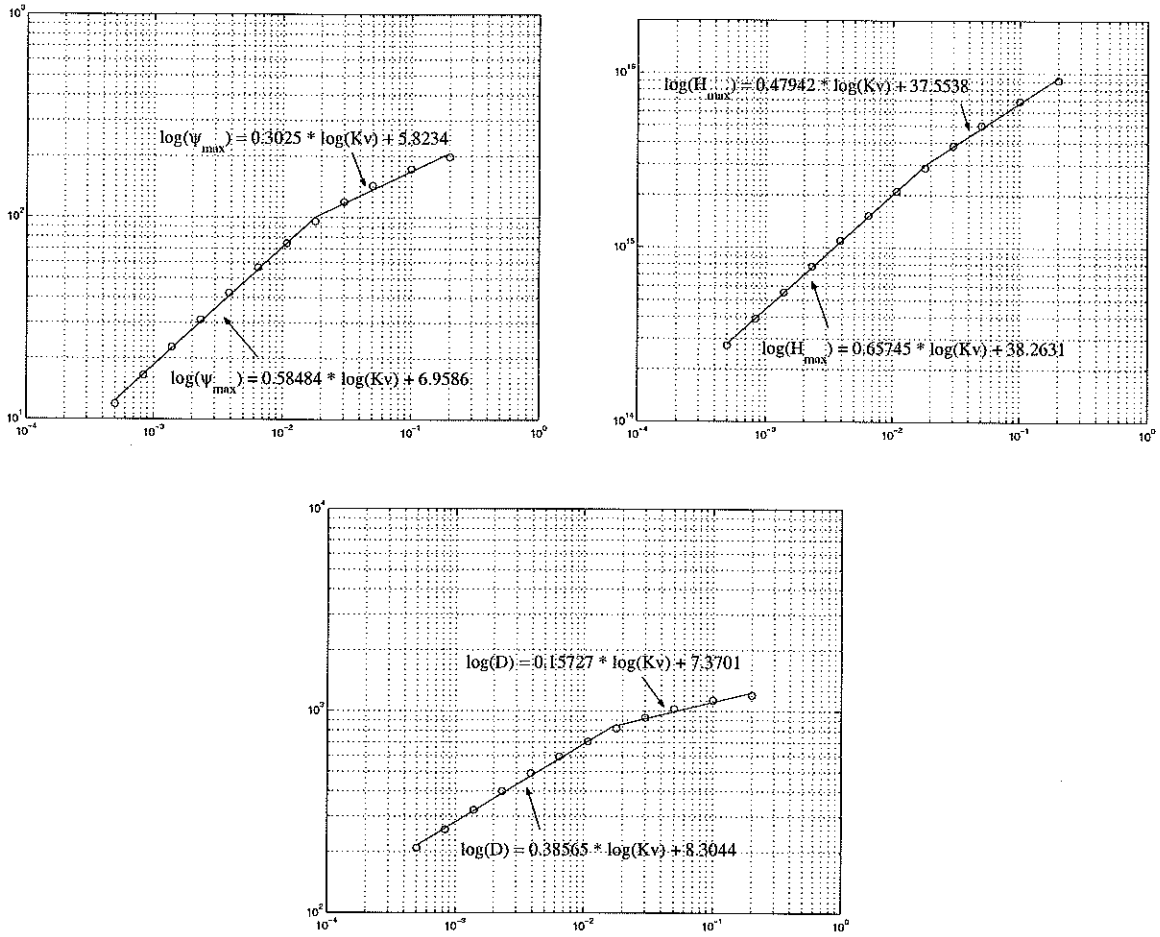

Figure 2.10: scale law over $K_v = 5 \sim 5000 \times 10^{-4} m^2 s^{-1}$. Two straight lines are least square fit. First fit is from $K_v = 5 \times 10^{-4} m^2 s^{-1}$ to $180 \times 10^{-4} m^2 s^{-1}$. Second fit is from $K_v = 180 \times 10^{-4} m^2 s^{-1}$ to $5000 \times 10^{-4} m^2 s^{-1}$. (a) A 2/3 power dependence of ψ_{max} on K_v from the first fit; (b) A 2/3 power dependence of maximum heat transport on K_v from the first fit; (c) A 1/3 power dependence of thermocline depth on K_v from the first fit.

2000)

$$D(y) = \frac{\int_{-H}^{0}(\rho - \rho_{bottom})zdz}{\int_{-H}^{0}(\rho - \rho_{bottom})dz} \tag{2.20}$$

This gives the average depth where the density gradient changes most. Fig 2.10(c) shows that the thermocline depth at $30°N$ scales as $K_v^{1/3}$.

2.3 Scaling analysis and discussion

From equations (2.9) and (2.10),

$$\frac{\partial W_W}{\partial z} + \frac{\partial W_E}{\partial z} = -\frac{\partial V_W}{\partial y} \tag{2.21}$$

$$\frac{W_W + W_E}{D} \sim -\frac{V_W}{L_y} \tag{2.22}$$

From thermal wind relation (2.6),

$$\frac{V_W}{D} \sim -\frac{g}{\beta y \rho_0}\frac{\rho_E - \rho_W}{\Delta x} \tag{2.23}$$

$$V_W \sim -\frac{Dg}{\beta y \rho_0}\frac{\rho_E - \rho_W}{\Delta x} \tag{2.24}$$

Where D is the scale of the depth of the thermocline.

Therefore,

$$\frac{W_W + W_E}{D} \sim \frac{Dg}{\beta y \rho_0 L_y}\frac{\rho_E - \rho_W}{\Delta x} \tag{2.25}$$

or

$$W_W + W_E \sim \frac{D^2 g}{\beta y \rho_0 L_y} \frac{\rho_E - \rho_W}{\Delta x} \tag{2.26}$$

From advective-diffusive balance,

$$W_W \sim \frac{K_v}{D} \tag{2.27}$$

$$W_E \sim \frac{K_v}{D} \tag{2.28}$$

$$W_W + W_E \sim \frac{2K_v}{D} \tag{2.29}$$

Eqn(2.26) and (2.19) can be combined into

$$W_W + W_E \sim \left[\frac{g}{\beta y \rho_0 \Delta x} \frac{\rho_E - \rho_W}{L_y} (2K_v)^2 \right]^{1/3} \tag{2.30}$$

$$D \sim \left[\frac{\beta y \rho_0 \Delta x}{g} \frac{L_y}{\rho_E - \rho_W} \right]^{1/3} (2K_v)^{1/3} \tag{2.31}$$

The meridional streamfunction and heat transport are scaled as

$$\psi = -\int W dx dy \sim \Delta x L_y (W_E + W_W) \sim \left[\frac{g}{f \rho_0} (\rho_E - \rho_W)(2\Delta x L_y K_v)^2 \right]^{1/3} \tag{2.32}$$

$$H = \int \rho c_p V T dx dz \sim \rho c_p \psi \Delta T \tag{2.33}$$

where c_p is the specific heat under constant pressure, ΔT is top-bottom temperature contrast.

With the surface forcing used in the numerical experiments, the surface density varies by about 6.15 kgm^{-3}. From Marotzke's theory (M97), the upper limit of $(\rho_E - \rho_W)$ is 1/4 of $(\rho_P - \rho_T)$. We use this value in our scaling analysis. With

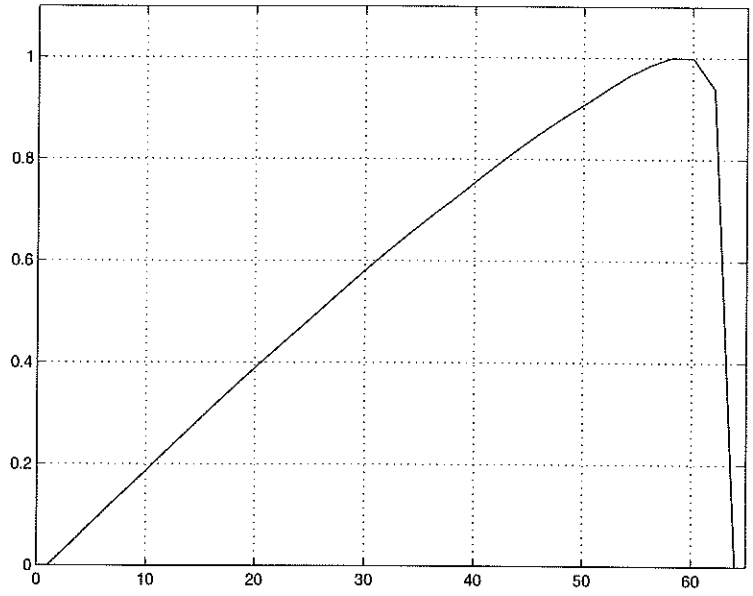

Figure 2.11: Latitudinal dependence of overturning from the numerical experiment with $K_v = 5 \times 10^{-4} m^2 s^{-1}$.

$\beta = 2 \times 10^{-11} m^{-1} s^{-1}$ and $L_y = 7004km$, this gives

$$\frac{g}{f\rho_0}(\rho_E - \rho_W) \sim \frac{1}{4}\frac{g}{\beta L_y \rho_0}(\rho_P - \rho_T) = 92ms^{-1} \tag{2.34}$$

with $K_v = 5 \times 10^{-4} m^2 s^{-1}$ and $\Delta x = 400km$,

$$(2\Delta x L_y K_v)^2 = 7.85 \times 10^{18} m^8 s^{-2} \tag{2.35}$$

This estimate yields the number $\psi_{max} = 9.0$ Sv. which is in good agreement with numerical results 11 Sv.

The latitudinal dependence of overturning from numerical results is plotted in Fig 2.11. This curve is normalized so that the maximum value is 1. This figure coincides with M97 (Fig.11(b) in his paper).

The overturning streamfunction and heat transport are thus intimately related

to east and west density difference by thermal wind balance. The magnitude and latitude of the maximum density difference didn't change much with K_v (fifth column of Table 1). Therefore, we can conclude meridional overturning strength is proportional to $K_v^{2/3}$. Notice that only the product $K_v \Delta x$ appears, indicating that K_v really is the diffusivity averaged over arbitrary boundary layer width Δx. Therefore only the zonal integral over the vigorously mixing region matters in the overturning streamfunction. We also plotted another climatically important diagnostic quality, meridional heat transport (Fig 2.10(b)). For meridional heat transport, a $K_v^{2/3}$ dependence is obtained.

The dependence of MOC and heat transfer on K_v are consistent with previous modeling studies (Park and Bryan 2000). The poleward heat transport is proportional to the meridional overturning rate multiplied by the temperature difference between the surface and deep water. Although the maximum of the MOC lies at high latitudes, the largest surface-deep water temperature difference appears at lower latitudes. Thus, the peak of poleward heat transfer is found in mid-latitudes. For our particular boundary conditions, surface density is prescribed, the temperature of deepest water is fixed and equals to that of polar water. Heat transport scales as overturning streamfunction ψ_{max}. In a later experiment, the surface boundary is relaxed. If relaxation time scale is short, an approximate $K_v^{2/3}$ of heat transport would be still valid. Park and Bryan(2000) indicated that for restoring boundary condition, we have to take into account that the top-to-bottom temperature contrast changes with K_v, the multiplication of ΔT and Heat(H) should scale as $K_v^{2/3}$, not H alone.

2.4 Summary

The simple numerical experiments reported here, rotating, two-dimensional, vertical mixing limited to both lateral boundaries, self-consistent, again were motivated by the fact that even the mixing is uniform, the vertical motion is closely confined to the lateral boundaries. The numerical results show good agreement with the results of 3-D GCM simulation by Marotzke (1997). The key factor of this simple model is the thermal wind balance on the rotating earth. The strength of ocean circulation is consequently linked to east and west density difference. The advantage of specifying two sidewall density explicitly is to avoid the need of closure assumptions entering two-dimensional models of THC. All previous attempts in 2-D model had to obtain a dynamical closure, which were based on ill-justified or empirical arguments. Although this model looks simple, we believe it captures a lot of basic physical features of THC, such as vertical mixing at the boundary, how it influences the density structure and therefore drives the large-scale circulation. It gives us a full appreciation of the influence that boundary mixing can have on the meridional overturning strength, thermocline depth, maximum stratification and poleward heat transport. It is not surprised that this model can predict most of patterns of OGCM quite well.

Newtonian damping surface condition gives surface temperature freedom to depart from the reference temperature(Park and Bryan 2000). Since the total equator-pole temperature difference is more important to determine the strength of overturning cell, it is a good strategy to analyze the scaling behavior using fixed surface temperature. In section 2.3, we showed both overturning streamfunction and heat transport behave proportional to $K_v^{2/3}$ over a broad range of vertical diffusivity. The overturning streamfunction depends very weakly on the shape of imposed thermal forcing. Because the vertical motions are assumed to concentrate near the boundaries, the traditional Stommel-Arons picture doesn't hold well. Particularly we found

that first the convection scheme is not necessary in the numerical computation; Secondly, the meridional overturning cell becomes shallower and has a narrow downward branch for small vertical diffusivity. The narrowness of deep sinking is a fundamental and ubiquitous characteristic of the buoyant overturning of the real ocean. I believe it is a measure of inefficiency of diffusive heat transport, the smaller vertical diffusivity is, the narrower and shallower the overturning cell would be. The explanation I provided is closer to Rossby's result (Rossby 1965). The argument in Marotzke and Scott (1999) is built in three dimensional frame work and can't be applied here.

Chapter 3

Model results in one-hemisphere under different surface conditions

3.1 Numerical experiments with different equator-pole temperature contrast

From the experiments in chapter 2, we emphasized that the THC is influenced by the imposed meridional density difference, not by the deep convection. In section 5, K_v is a constant $5 \times 10^{-4} m^2 s^{-1}$. In order to study the effect of equator-pole temperature contrast on THC, we explored $T_T - T_P$ at $20°C$, $30°C$, $40°C$ and $60°C$ respectively, with fixed polar temperature $0°C$. The strength of MOC is bounded up by east-west density difference. As discussed in M97, this in turn can be related by the equator-pole temperature contrast. These two density differences are proportional to each other and about the same magnitude (Bryan 1987), although Marotzke(1997) showed east-west density difference is a bit smaller. The equator-pole temperature contrast is a necessary gradient for a robust THC, that is why it is called buoyancy driven

circulation. We focus on the scaling behavior. The strength of MOC is proportional to $(\rho_T - \rho_P)^{1/3}$; The heat transport is proportional to $(\rho_T - \rho_P)^{4/3}$ (Fig 3.1), as consistent with our scaling analysis and thus indirectly confirmed Bryan's (1987) speculation (Eqn (2.32)). However, the results from this model are not the results from 3-D OGCM runs (Jeff Scott, personal communication). OGCM with similar boundary mixing and boundary conditions gave $(\rho_T - \rho_P)^{2/3}$ dependence of ψ. This may suggest that some important 3-D dynamics are not included in this model.

3.2 Numerical experiments with various surface density distribution

The ocean is in contact with atmosphere and forced from above. It is important to study the response of the ocean circulation to various shape of differential heating. Especially, we want to understand which part of temperature gradient at the surface more influence the ocean circulation. In this part, the surface density is imposed with various forcing, simulating the effect of different meridional density distribution. First, the surface density varies like cosine of latitude instead of linear function of latitude(dashed line in Fig 3.2(a)).

$$\rho_W(y,0) = \rho_E(y,0) = \rho_s(y) = \rho_P + (\rho_T - \rho_P)(1 + cos(\pi y/L_y))/2 \qquad (3.1)$$

The temperature in the low latitudes is higher than in the linear case, while the temperature in the high latitudes is lower. The temperature gradient in the mid-latitude is bigger than the linear surface gradient. The temperature contrast is more confined to the central part of the surface boundary. Therefore a fluid parcel will expose longer time to higher temperature before descending into the interior. This leads

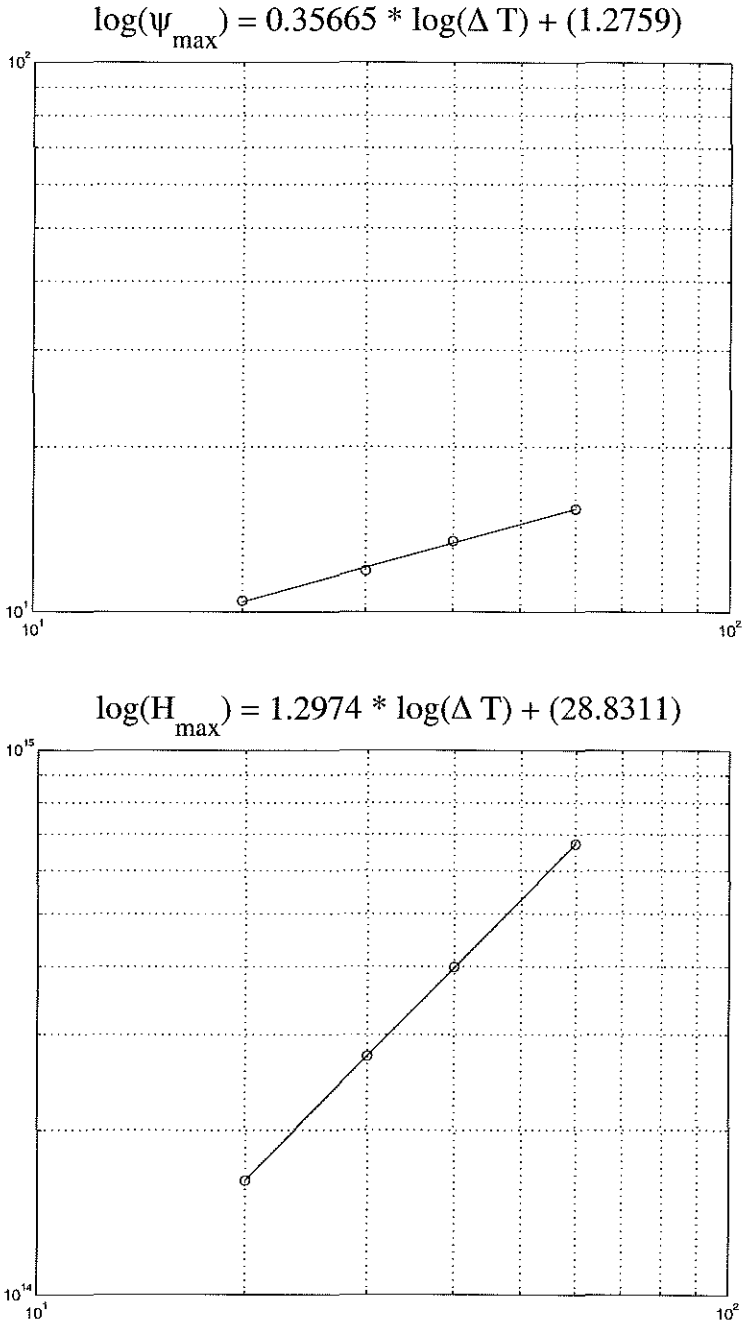

Figure 3.1: scale law for different equator-pole temperature contrast. The straight lines are least square fit. (a) A 1/3 power dependence of ψ_{max} on $T_T - T_P$; (b) A 4/3 power dependence of maximum heat transport on $T_T - T_P$.

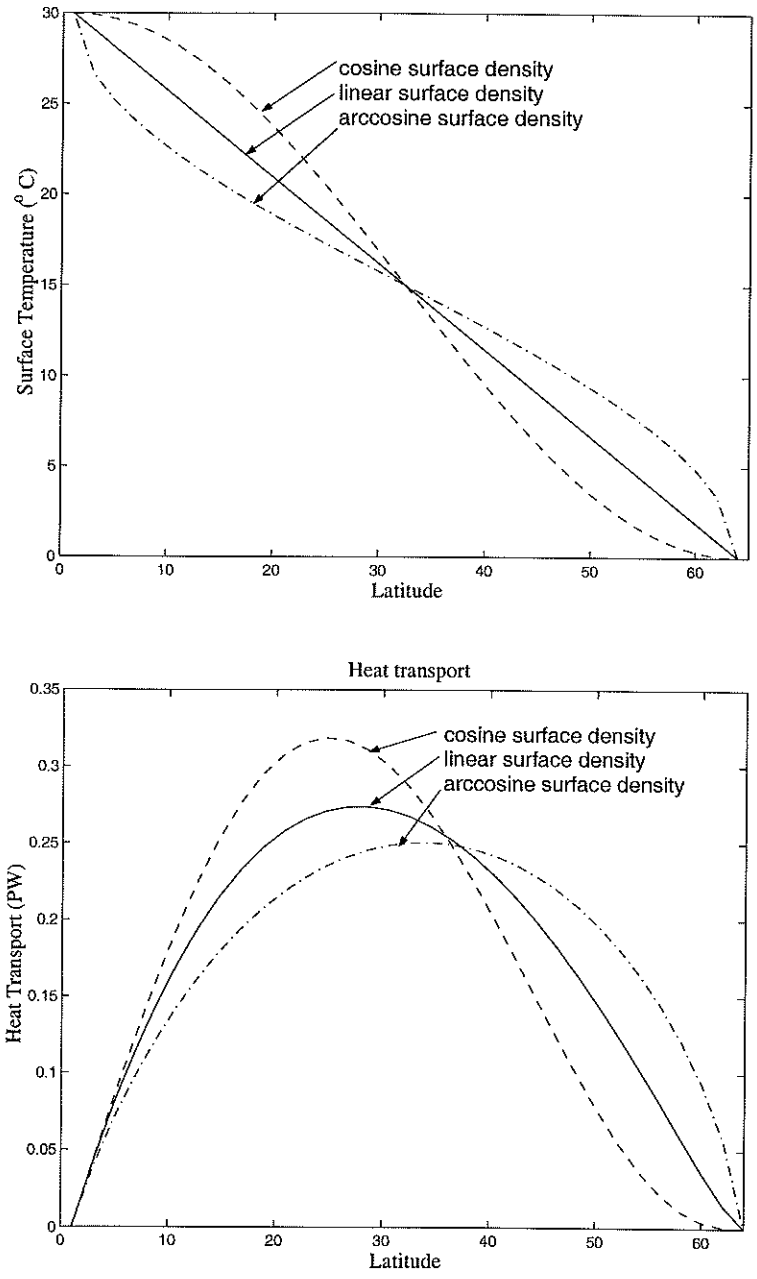

Figure 3.2: (a) Surface temperature profiles. (b) Heat Transport. Solid line: surface temperature is linear function of latitude; dash line: surface temperature is cosine function of latitude; dash-dotted line: surface temperature is arccosine function of latitude.

to higher interior temperature and increased efficiency of heat transfer. Similarly, longer exposure along the cold half improves the removal of heat. In addition, the heat transport is more concentrated in the central latitude as the meridional contrast is more concentrated to the center of the top. Its peak moves to the equator(dashed line, Fig 3.2(b)). The strength of the overturning for both surface conditions doesn't differ much. The maximum value of overturning only decreased 4%, about the same as linear case. The shape of MOC is similar (plot not shown).

Secondly, we tested the surface temperature profile with arccosine function as latitude (dash-dotted line, Fig 3.2(a)). In this case, comparing to the linear surface density distribution, the maximum value of overturning increased slightly. The heat transport becomes smaller and its peak moves poleward. It is obvious from this experiment that the meridional heat transport increases with mid-latitude temperature gradient. Scaling analysis showed that the strength of the meridional overturning is limited by the density difference between the eastern and western boundary, and by K_v as well. The magnitude of $\rho_E - \rho_W$ is proportional to $\rho_T - \rho_P$ (Marotzke 1997). Although the shape of imposed temperature is different between equator and pole, the strength of the circulation, which seems only care about overall equator-pole temperature difference, is much less affected.

It is instructive to see the response of the model to an extreme limit in surface temperature. The forcing surface temperature profile is a step function(Fig 3.3(a)), which corresponds to temperature gradient at mid-latitude is infinity (not so in numerical) and zero elsewhere. The equilibrium solution is shown in Fig 3.3(b)(c). Interesting enough, the strength of the overturning circulation hardly changes, but MOC confines itself in the low-latitude half of the basin. The downwelling happens at the location where the surface density is the same as abyss water (discussed in chapter 2). This argument can be seen more clearly from Fig 3.3(c), the site of downwelling is mid-basin instead of high latitude. The meridional heat transport is increased twice

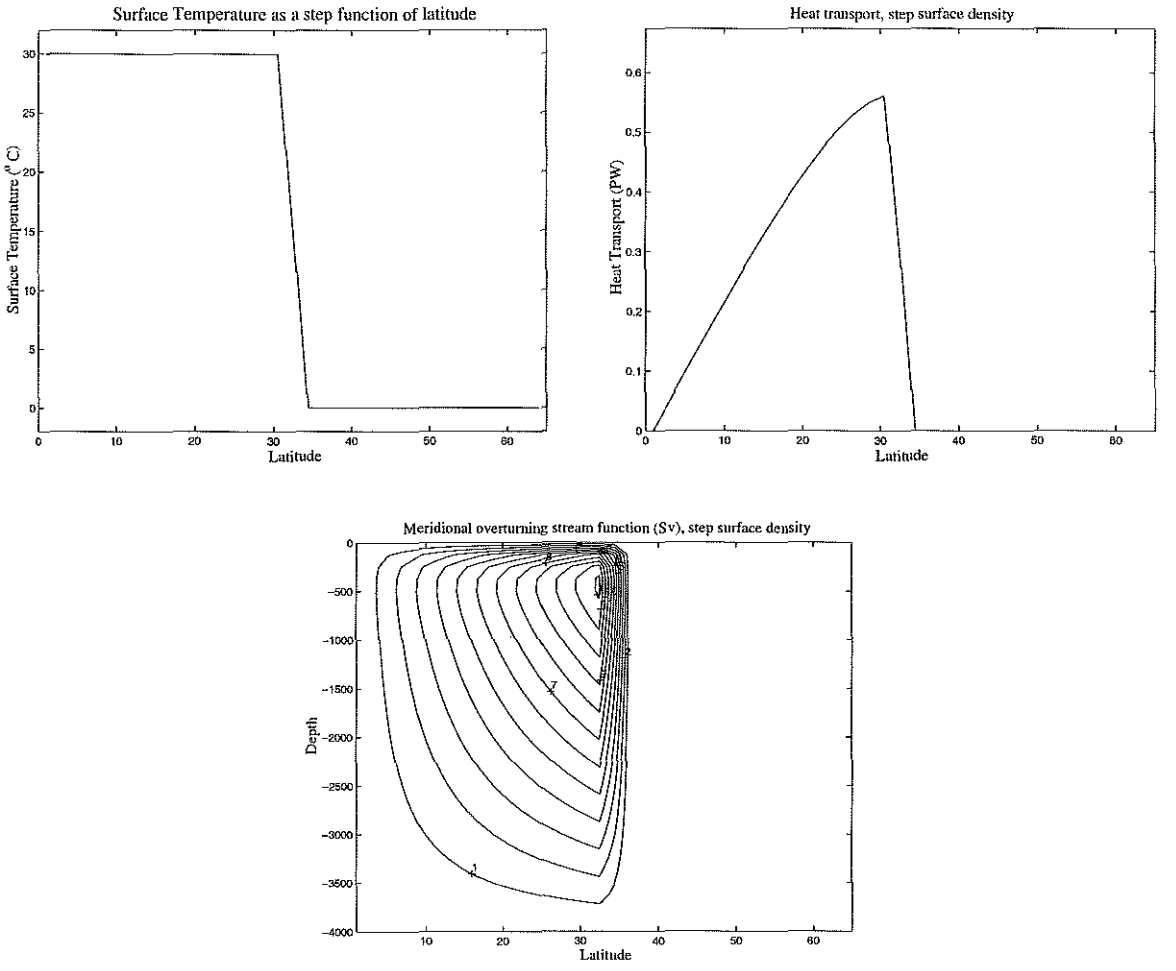

Figure 3.3: (a) surface temperature. (b) Heat Transport. (c) Meridional overturning streamfunction.

as much as in the case with linear surface temperature. Table 2 presents the results of this part.

Table 2. Summary of experiments with different surface temperature distribution

	ψ_{max} (Sv)	H_{max} (PW)
linear surface density	11.89	0.27
cosine surface density	11.37	0.32
arccosine surface density	12.97	0.25
step surface density	12.20	0.56

3.3 Numerical experiment with relaxation boundary condition

Instead of surface temperature fixed, the model now is relaxed to restoring boundary condition on temperature, the target profile is a linear function of latitude on western boundary layer (Eqn 2.1). The surface density of eastern boundary is inferred from western boundary when model reach equilibrium. An implication is that interior surface zonal flow is very efficient to transfer information from west to east boundary.(The more sensible run will be keeping surface density at eastern boundary fixed and only relaxing western boundary, which is not what I did). The abyssal water has property of coldest water and still kept fixed. (The reason is that when deep ocean is relaxed, there seems existing an oscillation solution. Whether it is a real oscillation is still under our investigation). As the first step in atmosphere-ocean coupling, we want to study how the surface heat flux change the results. The air-sea interfacial heat flux is parameterized by Newtonian law(Haney 1971). The heat transport and surface heat flux are diagnosed when the overturning streamfunction reaches equilibrium.

We make the simplifying assumption that the temperature is well mixed in the first level δ of the model. The surface heat flux into the ocean is approximated by a linear Newtonian law

$$Flux = \rho c_p \delta (T^* - T_o)/\tau \tag{3.2}$$

Where T_o is the ocean temperature, T^* is an apparent atmospheric temperature given. It is a linear function of latitude varying from $30°C$ at the equator to $0°C$ at the pole. The restoring time scale τ is the time scale of the air-sea interface heat exchange, we choose it as 30 days, which means the surface temperature is very nearly prescribed. δ is the depth of first level, which is 125 m; $\rho c_p = 4 \times 10^6 W m^{-3} K^{-1}$. The resolution again is 33×33 grid points.

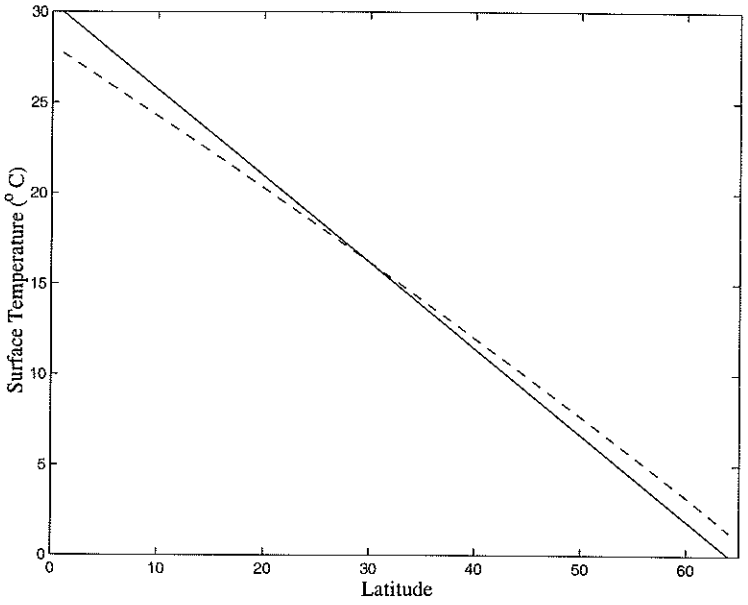
Surface Temperature (^{0} C)
Latitude
0
5
10
15
20
25
30
0
10
20
30
40
50
60

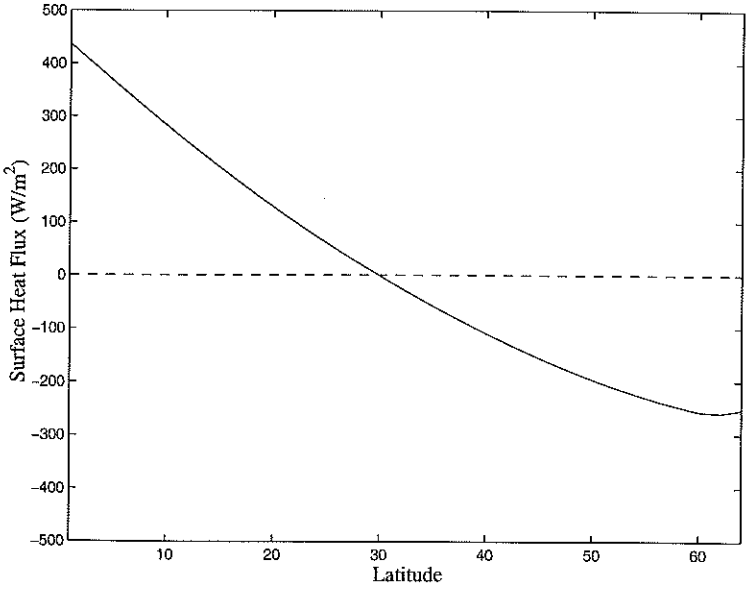
Surface Heat Flux (W/m^2)
Latitude
500
400
300
200
100
0
-100
-200
-300
-400
-500
10
20
30
40
50
60

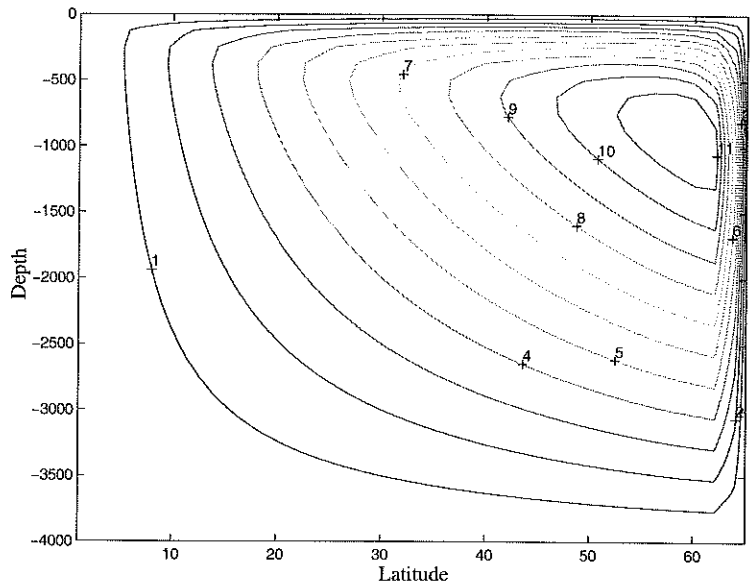

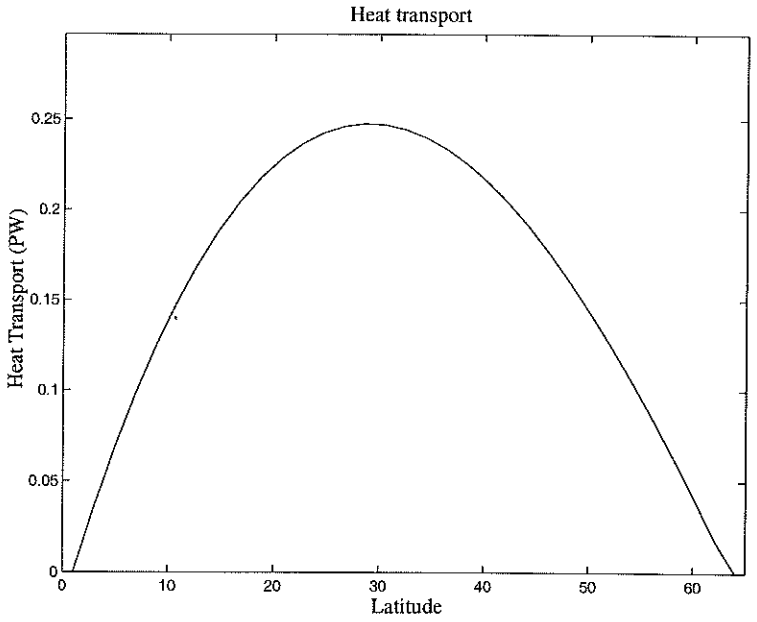

Figure 3.4: (a) Surface temperature; Solid line is the apparent atmosphere temperature, dash line is the relaxed ocean temperature. (b) Surface heat flux at western boundary; Dash line is zero heat flux. (c) Meridional streamfunction. (d) Heat Transport.

The circulation patterns obtained are very much similar to results in chapter 2. The surface temperature is relaxed (Fig 3.4(a)). At low (high) latitudes, the ocean surface is lower (higher) than atmospheric temperature right above it. Thus ocean absorbs heat from atmosphere in the tropics and releases heat at high latitudes. The total heat transport is slightly smaller than in fixed surface temperature (Fig 3.4(d)). Convection adjustment procedure is necessary and applied at western boundary only. This seems a little puzzling at first. Why convection adjustment scheme is not necessary in chapter 2, yet it is so crucial for numerical stability in the restoring boundary condition, especially along western boundary? The reason is rather numerical than physical. Under fixed boundary density, the densest water is at high latitudes. At western boundary, abyssal water temperature is fixed and the coldest, the local mixing will not produce unstable stratification. At eastern boundary, the strongest downwelling occurs at northeastern corner. The location of maximum surface density coincides with downwelling. The imposed deep boundary condition of temperature plays a 'substitute' role of convective mixing and therefore ensures a steady-state solution under fixed surface density. But when the surface density is relaxed as in this section, surface temperature at western boundary is changed by the surface flux, it is possible that the cold surface water is on top of the warmer one and becomes unstable. Thus the convective mixing adjustment procedure at western boundary is very crucial in obtaining a steady-state solution.

3.4 Summary

In section 3.3, the surface boundary is further relaxed. The resulting patterns are quite similar to those in section 3.2 and in chapter 2, except that the convection adjustment scheme need to be incorporated in the computation to suppress the numerical instability. This model differs very much with other 2-D models, because it

has two boundary layers and treats western boundary and eastern boundary specifically. Thus it enables us to investigate the role of convection mixing even in such a simple model. Under fixed surface boundary condition, strongest downwelling occurs at the same location as the coldest surface water and therefore produces a uniform water column, the overall effect on the circulation is as with convective mixing. On the other hand, under restoring boundary condition, the coldest surface water didn't co-locate with downwelling. The water will thus be unstably stratified. Convection adjustment scheme is important at western boundary layer.

Although the numerical experiments presented here can efficiently investigate the mixing along western and eastern boundaries, it can not predict ocean circulation with enhanced diffusivity at other boundaries or in localized interior regions. Details of the resulting solutions will depend strongly on the distribution of the mixing region. Over a broad domain of vertical diffusivity, this quasi 2-D model didn't exhibit the oscillation solution for the meridional overturning stream function, nor did it result a thermally indirect cell as observed in some OGCM runs, even when the vertical diffusivity was increased to 1000 or $10,000 \times 10^{-4} m^2 s^{-1}$. All experiments reported so far were performed with surface density prescribed or nearly so. It is very likely, however, that the scaling behavior and pattern change as the experiments use more realistic atmosphere coupling, for example, if abyssal ocean is relaxed. This model doesn't include a lot of three dimensional dynamics, some results obtained are not consistent with OGCM results (section 3.1). The wind stress is totally omitted, isopycnals are flat along the equator and between the western boundary current and the eastern wall. These simple assumptions are enforced to abandon if the surface wind is added and wind-driven thermocline structures may change the pictures reported here.

Chapter 4

Extended simplified dynamical model in 2-hemisphere, 1-basin system

4.1 Circulation pattern in the global THC

An important feature of the global THC is characterized by a unidirectional deep mass transport in two hemispheres (Macdonald and Wunsch 1996; Ganachaud 1999). In order to support deep southward meridional velocity, the zonal density gradient needs to change sign across the equator. How and why the ocean reaches this state is very interesting to understand oceanic dynamics. Previous OGCM results suggest that the global deep water formation rate is constrained by the average pole-equator density difference (Tziperman 1997; Wang et al. 1999; Marotzke 1999). There are several possibilities for the partition of deep sinking in the North Atlantic and Southern Ocean. Tziperman (1997) found that the NADW formation rate is sensitive to the

restoring surface salinity profile in the northern high latitudes. Wang et al (1999) showed that the magnitude of the global freshwater flux governs the partition. In our dynamical model, we will show the partition is mainly controlled by high latitude density difference in our temperature-only model.

Many 3-D studies in the ocean general circulation model (OGCM) suggested that the THC strength in the North Atlantic in a two-hemisphere single basin system is governed by the pole-to-pole overturning dynamics (Hughes and Weaver 1994; Rahmstorf 1996). Hughes and Weaver (1994) used OGCM and found a linear relation between overturning strength and the difference in vertically integrated steric height (a measure of depth-integrated pressure). Two recent works by the same authors, Klinger and Marotzke (1999) and Marotzke and Klinger (2000, hereafter MK00), confirmed Hughes and Weaver's result. Further they found that small pole-to-pole temperature differences could set up a markedly asymmetric THC and therefore manifest the amplification of small density asymmetries into large overturning asymmetries. These seems like robust features in the global THC. Part of our motivation is to reproduce these circulation patterns in our simple model and to give them simple dynamical explanation.

4.2 Extended simplified dynamical model in 2-hemisphere

The dynamical model in 1-hemisphere is tested successfully (the equator is avoided intentionally in Chapter 2 and 3). However in two-hemisphere, the geostrophic equations right at the equator is singular. To compensate for the lack of Coriolis terms, Rayleigh friction terms are introduced into the thermal wind equation as dissipative agents. This has been used by Gill (1982), Huang and Yang (1996). A Rayleigh frictional damping term is included in the geosptrophic equation to overcome the

singularity of Coriolis terms. The equations in assumption $i), ii), iv), vi)$ and $vii)$ in chapter 2 remain the same. It is worthwhile to restate the assumption $i)$ in double-hemisphere.

$i)$ Surface density is given and is a function of the latitude only in either hemisphere.

In Northern Hemisphere,

$$\rho_W(y,0) = \rho_E(y,0) = \rho_s(y) = \rho_N + (\rho_T - \rho_N)(1 - y/L_y) \tag{4.1}$$

In Southern Hemisphere,

$$\rho_W(y,0) = \rho_E(y,0) = \rho_s(y) = \rho_S + (\rho_T - \rho_S)(1 - y/L_y) \tag{4.2}$$

Where ρ_N and ρ_S are the surface density at the northern wall and southern wall respectively.

$i)$ Unlike the assumption in 1-hemisphere, the abyssal water property could be influenced by densest surface water at both hemispheres. In one-hemisphere model, we have seen that the coldest surface water through downwelling at the north-eastern corner sets the abyssal water temperature. In double hemisphere, the abyssal water properties are unknown. It is not clear how the coldest surface water determines the abyssal water temperature in double-hemisphere. This assumption is very crucial because this model is very sensitive to the bottom water condition. Non-heat flux condition is then used in numerical calculation. For sensitivity study purpose, the deep water is later fixed to be the coldest surface water. Although the latter assumption is not realistic, it indeed tells us some aspects of this model.

v) The modified equations of assumption $iii), v)$ are as follows.

$$-fV_W = -\frac{1}{\rho_0}(\partial_x P - rU) \tag{4.3}$$

$$fU = -\frac{1}{\rho_0}(\partial_y P - rV_W) \tag{4.4}$$

Where P represents the pressure difference, r is on the order of $\beta y \sim 10^{-5}s^{-1}$.

From Eqns 4.3 and 4.4, we get

$$V_W = \frac{1}{\rho_0(f^2+r^2)}(f\partial_x P - r\partial_y P) \tag{4.5}$$

$$U = -\frac{g}{\rho_0(f^2+r^2)}(f\partial_y P + r\partial_x P) \tag{4.6}$$

Then the thermal wind relations are obtained in double hemisphere.

$$\partial_z V_W = -\frac{g}{\rho_0(f^2+r^2)}(f\partial_x \rho - r\partial_y \rho) \tag{4.7}$$

$$\partial_z U = \frac{g}{\rho_0(f^2+r^2)}(f\partial_y \rho + r\partial_x \rho) \tag{4.8}$$

Where $\partial_x \rho = \frac{\rho_E - \rho_W}{\Delta x}$, $\partial_y \rho = \frac{\partial \rho_E}{\partial y}$ for the conciseness of the notation.

Through above equations plus the unchanged assumption in one-hemisphere, a set of more complicated equations are further derived:

$$\partial_{zz}W_W = \frac{g}{\Delta x\rho_0(f^2+r^2)^2}[\frac{\rho_E-\rho_W}{\Delta x}(-\Delta x\beta^3y^2+\Delta xr^2\beta-r^3-r\beta^2y^2)$$
$$+2r\Delta x\beta^2y\partial_y\rho_E+(-\beta^3y^3-r^2\beta y)\partial_y\rho_W+(-r\Delta x\beta^2y^2-r^3\Delta x)\partial_{yy}\rho_E] \tag{4.9}$$

$$\partial_{zz}W_E = \frac{g}{\Delta x\rho_0(f^2+r^2)}(r\frac{\rho_E-\rho_W}{\Delta x}+f\partial_y\rho_E) \tag{4.10}$$

Again all the equations were discrete using finite difference methods. Except modifying some dynamics at the equator, the basic assumptions of one-hemisphere remain untouched. The domain extends from 64° north to 64° south. The bottom of the basin is at a constant depth of 4000m. The width of two boundary layers at western and eastern boundary Δx is chosen as 400km. Static instability is removed by a convective adjustment procedure. The vertical diffusivity K_v is set to $5\times10^{-4}m^2s^{-1}$ inside side walls.

4.3 Numerical results

4.3.1 Asymmetric equilibrium

We introduce a surface forcing asymmetry about the equator by increasing the target SST profile by 1° at the Southern boundary (Fig 4.1). The model starts from an equilibrated run without the SST asymmetry. To speed up the time to reach a new equilibrium, the water is initially prescribed as exponentially decayed with the depth. We will refer the new equilibrium state as 'standard run'.

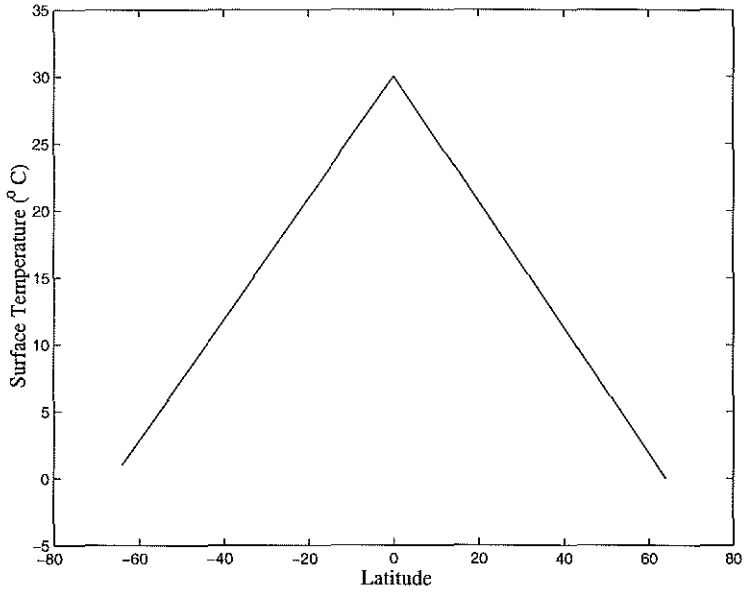

Figure 4.1: Surface temperature. At northern hemisphere, it linearly decreases from $30°C$ at the equator to $0°C$ at the pole. At southern hemisphere, it linearly decreases from $30°C$ at the equator to $1°C$ at the pole.

Fig 4.2 displays the steady state temperature at the western and eastern wall is very nearly symmetric about the equator. However the meridional overturning stream function shows a very strong asymmetry (Fig 4.3(b)). The amplification of small density asymmetries into large overturning asymmetries is a prominent feature of the global THC (Cox 1989; Marotzke and Willebrand 1991; Klinger and Marotzke 1999; Marotzke and Klinger 2000). This picture is consistent with these previous studies.

In the standard run, there is about 6.5 Sv crossing the equator, a maximum at North of 15.2 Sv, and a minimum of 9.0 Sv sinking at South. The sum of the overturning stream function over both hemisphere is about the same as in the symmetric solution, which is 12 Sv in both hemisphere. The global deep water formation is constrained by the overall vertical diffusive heat flux (Munk and Wunsch 1998, MK00). The vertical diffusive heat flux is mainly a function of diffusivity, hence the overturning strength is similar in symmetric and asymmetric experiments. This is

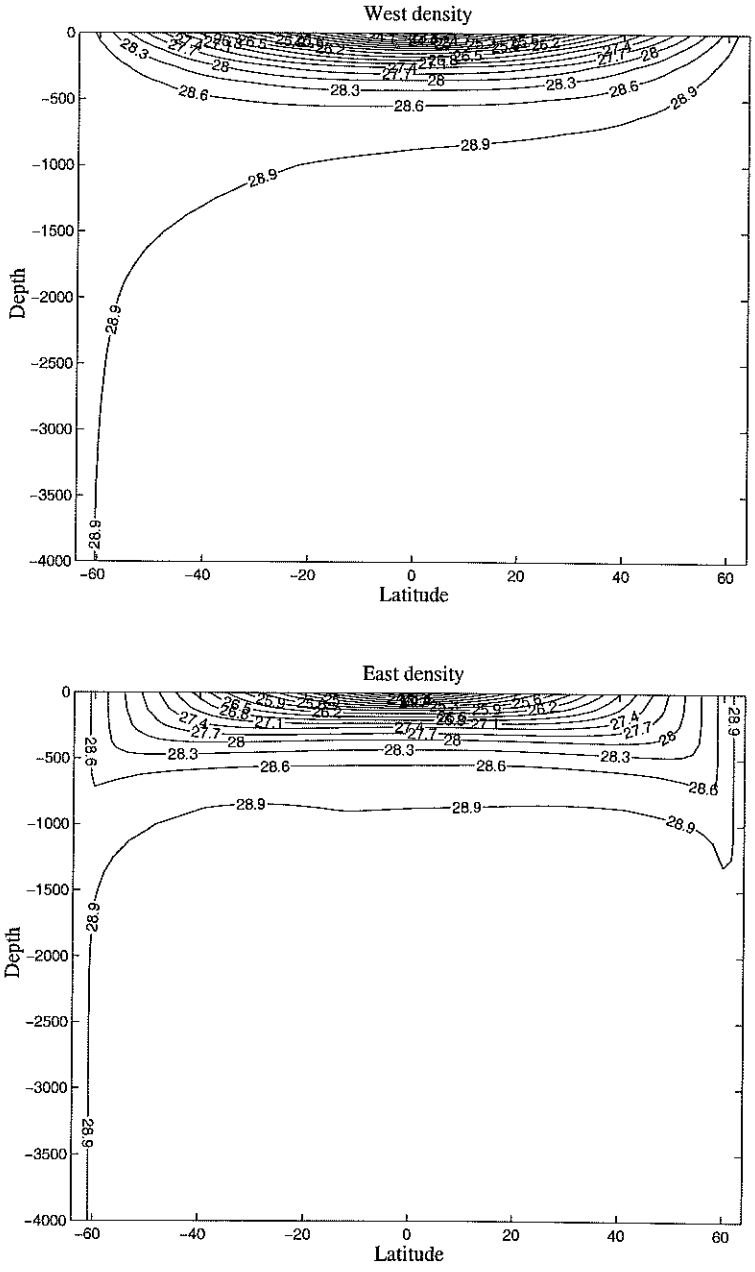

Figure 4.2: (a) Western boundary density in double hemisphere. (b) Eastern boundary density in double hemisphere. Contour interval $0.2kgm^{-3}$.

verified by numbers of other model studies in one-hemisphere sector ocean (Bryan 1987; Park and Bryan 2000; Zhang et al. 1999).

Comparisons of Fig 4.3 and Fig 4.4 results show the resemblance to MK00's 3-D OGCM results. Fig 4.3 (a) shows the density difference at the eastern and the western boundaries. The resulting THC (Fig 4.3(b)) has the right order of magnitude, but its structure is not very satisfactory; for example, the overturning cell in the SH (dashed line in Fig 4.3(b)) is extended to the bottom even at the large pole-to-pole temperature contrasts. In the OGCM, the SH overturning cell is nearly confined to the upper part of the ocean (Fig 4.4(b)). This is probably due to the thermal structure at the abyss. A sensitivity study is conducted to illustrate this point in the following subsection. buoyancy

4.3.2 Mechanism for the asymmetry of the overturning stream-function

Above we found that very small pole-to-pole surface density differences could set up a markedly asymmetric THC in our simple model. The fundamental cause lies in the weak abyssal stratification, as pointed out by MK00. A $1°C$ temperature difference represents a vertical depth of 1-2 km in the deep ocean. Therefore a significant portion of the ocean volume is inaccessible to the 'lighter' source, since the denser water will fill up big part of the abyss. Asymmetry of the THC about the equator is arised because of asymmetric forcing.

One characteristic of Asymmetric THC is the unidirectional deep meridional transport geostrophically. This is shown in Fig 4.5. In order to support geostrophic balance of deep unidirectional transport, the deep pressure difference between eastern and western boundaries must change sign at the equator. Fig 4.3 (a) illustrates how

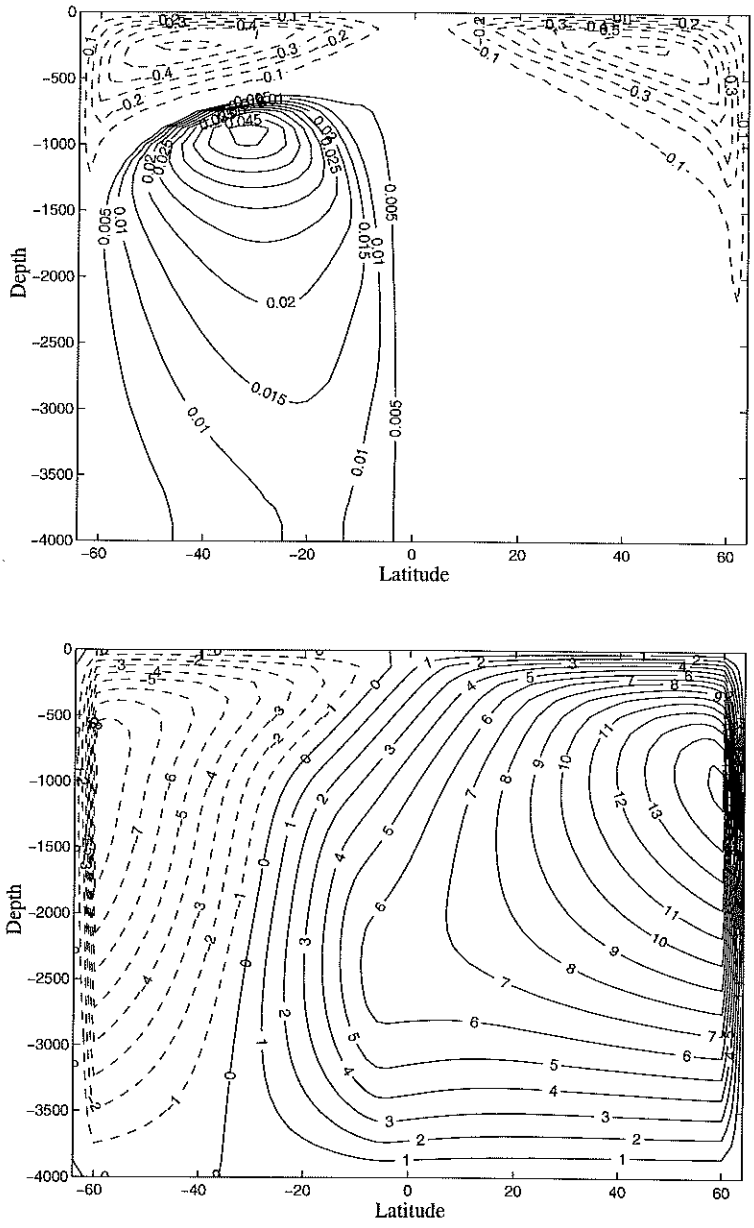

Figure 4.3: (a) Density difference as eastern wall minus western wall. Solid line: positive, contour interval $0.005 kgm^{-3}$; dash line: negative value, contour interval $0.1 kgm^{-3}$. (b) Meridional streamfunction, the flow field is clockwise around the positive value, anticlockwise around the negative value. Contour interval 1 Sv.

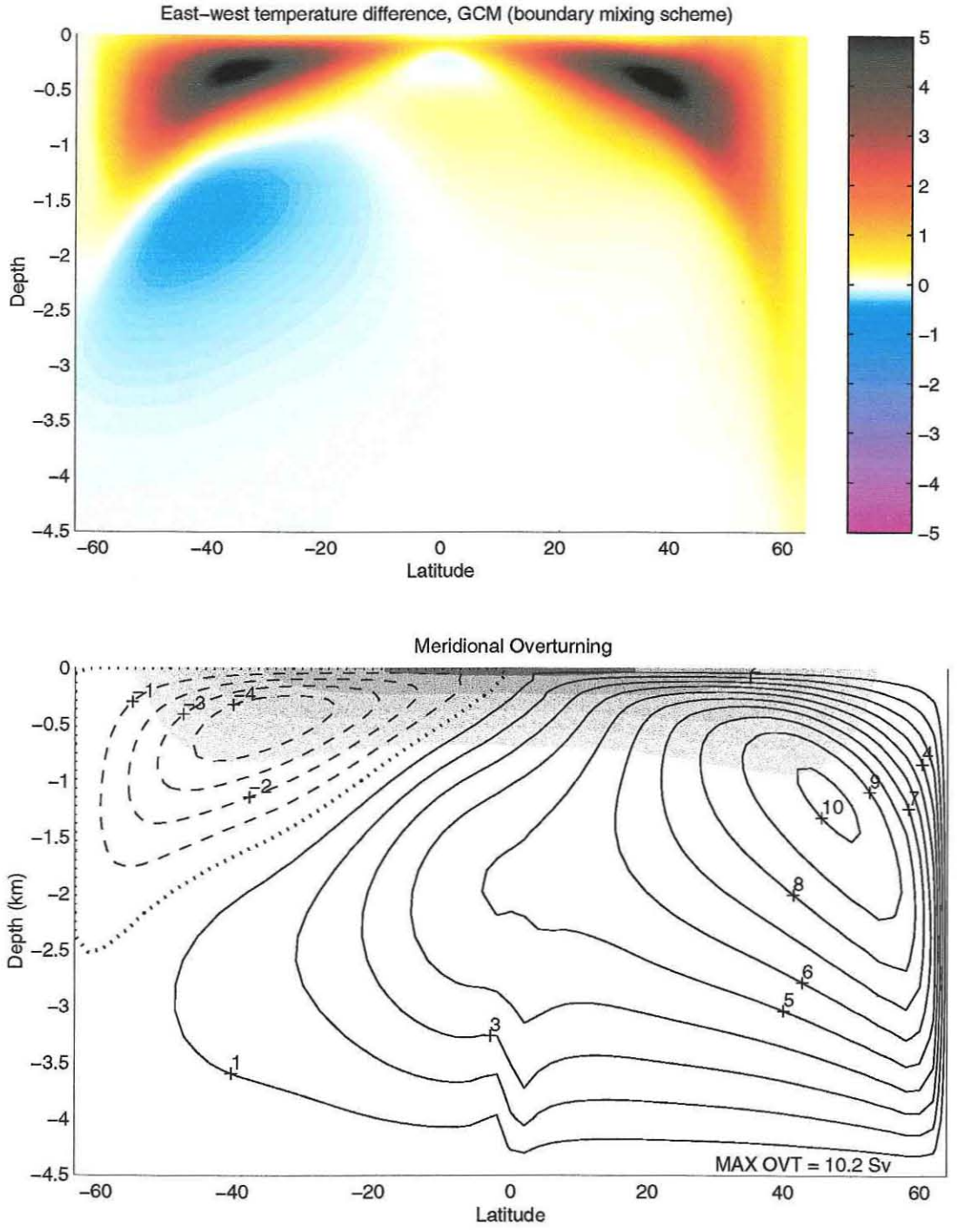

Figure 4.4: (a) Temperature difference, eastern boundary minus western boundary. The magnitude of temperature is indicated by the side color bar. Density is a linear function of temperature and is represented by temperature. (b) Meridional streamfunction, the flow field is clockwise around the positive value, anticlockwise around the negative value. Contour interval 1 Sv, the zero contour is dotted. Pictures are from Jeff Scott's 3-D numerical results, which used better numerical scheme than Marotzke and Klinger 2000, the results are nevertheless very close.

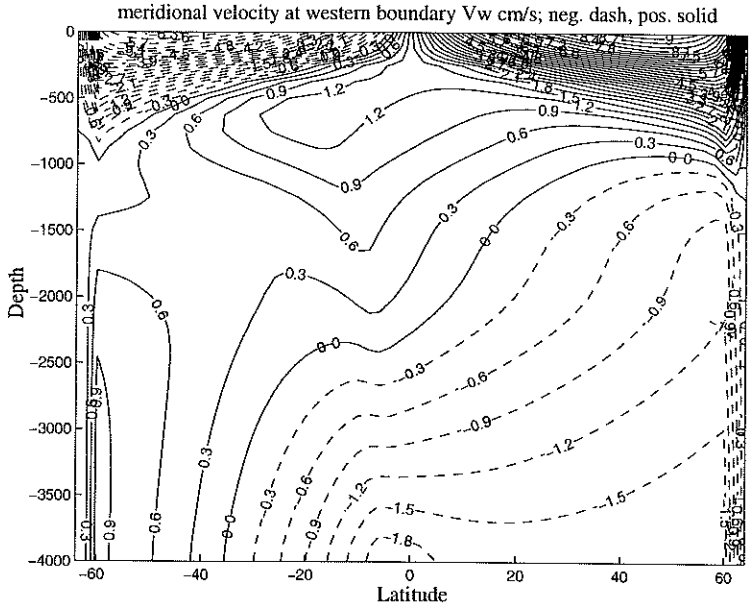

Figure 4.5: Meridional velocity at western wall, contour interval $0.3cms^{-1}$. Solid line: positive; dash line: negative value.

this pressure difference is set up by the density difference between eastern and western walls. The *thermocline* east-west density differences are nearly symmetric about the equator. However the *deep* east-west density differences strongly asymmetric about the equator, with reversal near the equator.

How the ocean reaches this state in double hemisphere is very intriguing. M97 and MK00 first developed theoretical concepts to understand what sets up the mean zonal pressure (or the density) gradient, which geostrophically balances the thermally direct THC cell in one hemisphere, and unidirectional deep thermohaline transport in two hemispheres. In particular, MK00 provided a reasonable explanation on how the deep zonal-mean zonal pressure gradient reverses at the equator in order to support deep southward transport. They conducted a spin-up experiment starting from a symmetric MOC in both hemispheres; asymmetric surface forcing is applied, with lighter surface density in the southern hemisphere.

In their spin-up experiments in MK00, the authors argued that the time scale

for a deep density anomaly to reach the equator is set up through the advection by the mean deep western boundary current, which is on the order of several decades. This time scale is much larger than the propagation time set up by Kelvin waves or 'boundary waves' (Kawase 1987; Killworth 1985), which is on the order of several months. It is not clear which of these various plausible time scales, ranging from months to decades, is more relevant. Nevertheless, the propagation pattern of the deep cold anomaly is similar in MK00 and Kawase 1987. The deep anomaly starts from the north-western corner, propagates along the western boundary southwards. When it gets the equator, it turns around and propagates along the equator till it meets the eastern boundary. Then it will in both directions along the eastern boundary.

This process is very important to set up the deep water temperature. As a result of path of deep anomaly propagation, the western boundary in the Southern Hemisphere is isolated from the rest of the ocean. Hence the deep water at the western boundary in SH is relatively warmer than those at the eastern boundary in the SH. Fig 4.6 displays a very interesting feature of abyssal water. In the northern Hemisphere, the water at the western boundary is colder than ones at the eastern boundary. This verifies that downwelling process at the eastern boundary brings down warm water from the surface. It acts as a buoyancy source (Marotzke and Scott 1999). In the southern hemisphere, on the contrary, the water at the western boundary is warmer than ones at the eastern boundary. This is mainly due to the path of the propagation of the deep cold anomaly during the spin-up. Water at the eastern boundary in SH is affected by cold anomaly from Northern Hemisphere. The deep SH western boundary is on the other hand, isolated from reach of this cold anomaly.

The abyssal water properties, which are shown from the spin-up process, are the key to understand the zonal density difference between eastern and western walls. Recall in chapter 2, in our 1-hemisphere runs, the eastern boundary is lighter than the

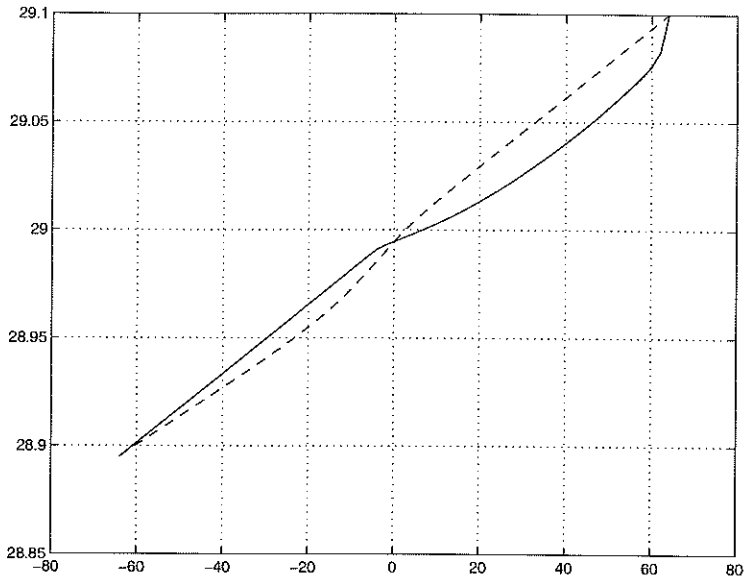

Figure 4.6: Density of two boundaries at the bottom 4000 km as function of latitude. Solid line: density at the western boundary. Dash line: density at the eastern boundary.

western boundary throughout the total depth, as is in the NH in double-hemisphere runs (Fig 4.3(a)). In SH, near the surface, the buoyancy source of downwelling still exists, hence the eastern boundary is warmer than the western boundary inside the thermocline. However the abyssal eastern boundary is colder than the western boundary, the east-west density difference reverses sign at some finite depth above the bottom.

In addition, the anomalous warm deep western density in SH creates the circulation pattern looks very different from NH. The vertical velocity at the SH western wall is downwelling at the depth, contrast to upwelling everywhere in the NH (Fig 4.7(a)). The result is very similar to OGCM results (Fig.4 in MK00, reproduced in Fig 4.8(a)). In order to maintain the deep warm anomaly, the source for the buoyancy is necessary. The downwelling in the SH western boundary plays this role and warm water which downwells from the thermocline into the abyss. Notice this phenomenon is ubiquitous in both hemisphere. Downwelling makes the NH eastern boundary warmer than NH western boundary as we notice in 1-hemisphere experiments.

A comparison of Fig 4.7(b) with OGCM results (Fig 4.8(b)) shows their difference. Vertical velocity at SH eastern boundary is very strong in Fig 4.7(b). It is very different from the GCM results (Fig 4.8(b)), where the vertical velocity is nearly symmetric, equatorward about 48° latitude. In our simple dynamical model, the interior flow is assumed purely zonal. The downwelled motion at the SH deep western boundary push water moving eastward (Fig 4.9). Because of lack of the interior re-circulation (i.e. meridional velocity), all the pushed eastward water has to upwell at the eastern boundary, which causes very strong upwelling in our model.

4.4 Sensitivity study

4.4.1 Sensitivity to equatorial condition *iii*)

We used the assumption *iii*) (as in chapter 2) in above calculations and forced the density at two boundary equal to each other at every time step. This assumption turns out not to be necessary. The steady state solutions are virtually the same as in section 4.2 (pictures are not shown). Even though the equator is not forced, the model seems to adjust itself to generate similar patterns. The following scaling analysis suggests that when Rayleigh friction is included, the governing equations expect the equatorial western and eastern boundary density become very close.

The final equations for eastern vertical velocity We and western vertical velocity Ww are:

$$\partial_{zz} W_E = \frac{g}{\Delta x \rho_0 (f^2 + r^2)} (r \frac{\rho_E - \rho_W}{\Delta x} + f \partial_y \rho_E) \tag{4.11}$$

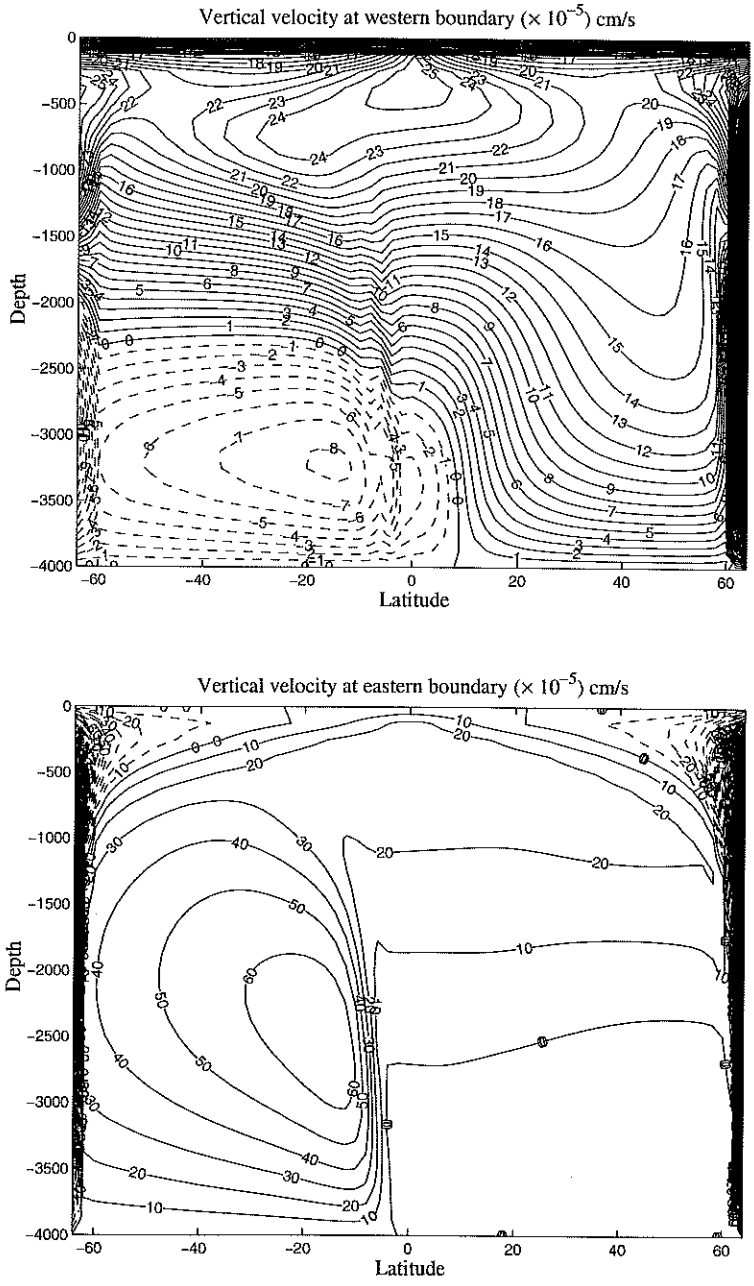

Figure 4.7: (a) Vertical velocity at western boundary, contour interval $1 \times 10^{-5} cms^{-1}$. (b) Vertical velocity at eastern boundary, contour interval $10 \times 10^{-5} cms^{-1}$.

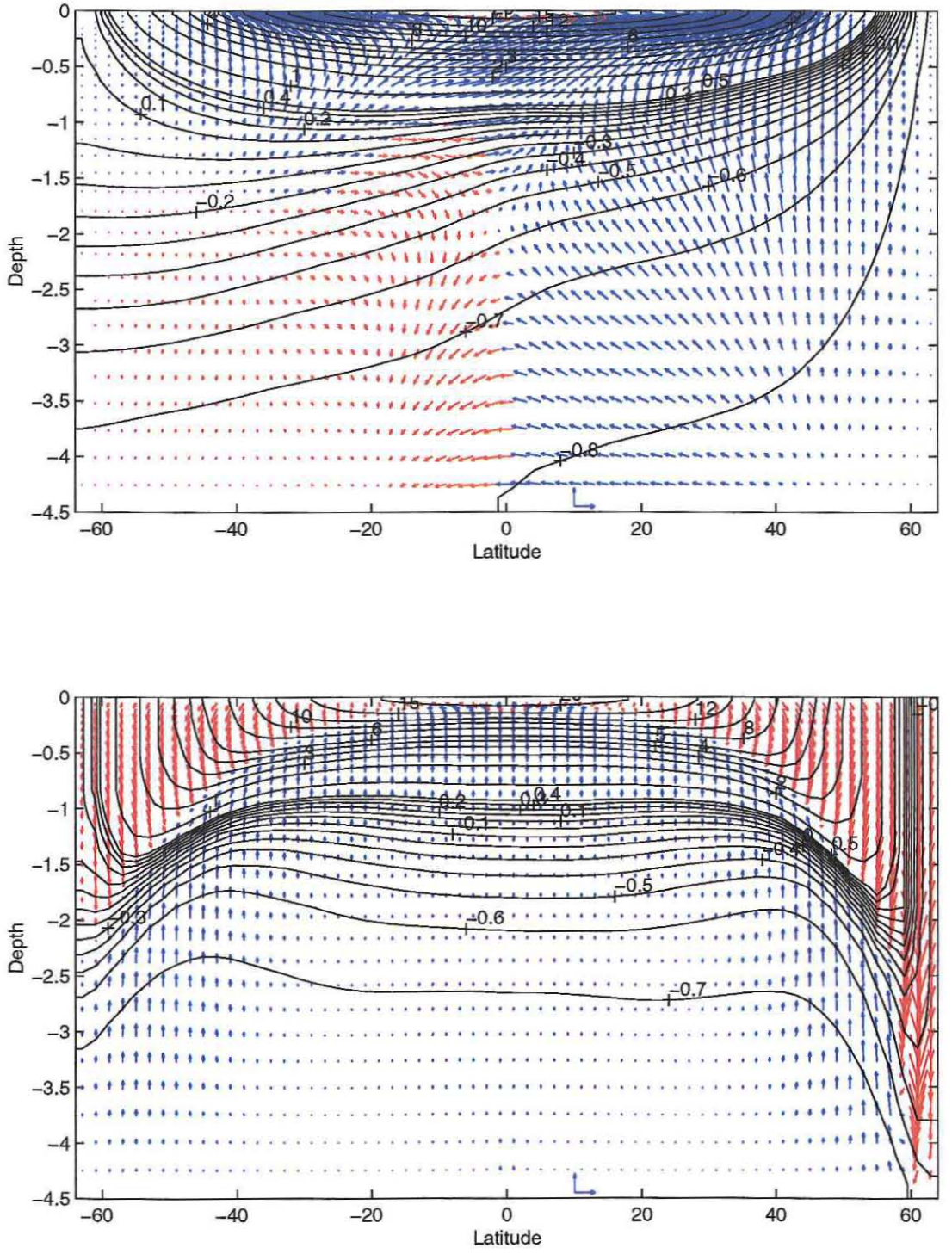

Figure 4.8: (a) Vertical velocity at western boundary, indicated by arrows. (b) Vertical velocity at eastern boundary, indicated by arrows. The reference velocity scale is shown by a tiny coordinates in the deep ocean. Reference upward velocity scale is $10 \times 10^{-4} cms^{-1}$. Reference horizontal velocity scale is $2 cms^{-1}$. Red color show the upwelling motion. Blue color shows the downwelling motion. Reference horizontal velocity scale is $2 cms^{-1}$. Solid lines are temperature contours along western boundary, magnitude is as marked. Pictures are from Jeff Scott's 3-D numerical results.

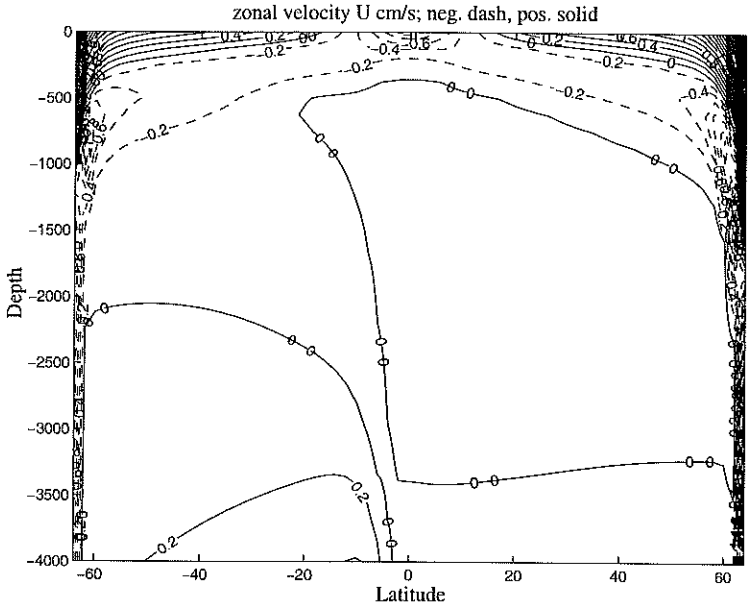

Figure 4.9: Zonal velocity, contour interval $0.2cms^{-1}$. Solid line: positive; dash line: negative value.

$$\partial_{zz}W_W = \frac{g}{\Delta x\rho_0(f^2+r^2)^2}[\frac{\rho_E-\rho_W}{\Delta x}(-\Delta x\beta^3y^2+\Delta xr^2\beta-r^3-r\beta^2y^2) +2r\Delta x\beta^2y\partial_y\rho_E+(-\beta^3y^3-r^2\beta y)\partial_y\rho_W+(-r\Delta x\beta^2y^2-r^3\Delta x)\partial_{yy}\rho_E] \tag{4.12}$$

At the equator, $f=0$, $y=0$, the equation simplifies to

$$\partial_{zz}W_E = \frac{g}{\Delta x\rho_0 r}(\frac{\rho_E-\rho_W}{\Delta x}) \tag{4.13}$$

$$\partial_{zz}W_W = \frac{g}{\Delta x\rho_0 r^2}[\frac{\rho_E-\rho_W}{\Delta x}(\Delta x\beta-r)-r\Delta x\partial_{yy}\rho_E] \tag{4.14}$$

The scaling analysis of above two equations gives:

$$\frac{W_E}{D^2} \sim \frac{g}{\Delta x^2 \rho_0 r}(\rho_E - \rho_W) \tag{4.15}$$

$$\frac{W_W}{D^2} \sim \frac{g}{\Delta x^2 \rho_0 r^2}[(\rho_E - \rho_W)(\Delta x\beta - r) - r\Delta x^2 \frac{\rho_E}{L_y^2}] \tag{4.16}$$

Where L_y is the scale of the longitudinal width.

Adding two above equations up,

$$\frac{W_W + W_E}{D^2} \sim \frac{g}{\Delta x \rho_0 r^2}[(\rho_E - \rho_W)\beta - r\Delta x \frac{\rho_E}{L_y^2}] \tag{4.17}$$

From vertical advection-diffusion balance,

$$W_W + W_E \sim \frac{2K_v}{D} \tag{4.18}$$

Manipulating the equations, we have

$$\rho_E - \rho_W \sim \frac{1}{\beta}(\frac{2r^2 \Delta x \rho_0 K_v}{gD^3} + \frac{r\Delta x \rho_E}{L_y^2})$$

The density difference between both boundaries is proportional to r^2 and r. As long as Rayleigh friction r is very small, the density difference at the equator is close to zero. We gave r value of $5 \times 10^{-6} s^{-1}$ through all the runs.

4.4.2 Sensitivity to abyss condition *i)*

The circulation of the ocean is expected very sensitive to the deep water boundary condition. In previous subsection, the boundary condition we used is non-heat flux,

which is a very good assumption in the deep ocean. Supposely, if there is geothermal source for mixing (Huang 1999), this will change the bottom boundary condition and large-scale circulation correspondingly (Jeff Scott, personal communication). We will consider an extreme case where the deep ocean keep the coldest possible surface water, which is 0° degree from at the Nothern pole. This bottom comdition dramatically change the whole pattern.

The results from this experiment are not completely included here. Basically, the western-eatern density difference and the overturning ciculation are almost symmetric (Fig 4.10). Very unlike the previous case, where the small change at the surface causes a big shift of the overturning cell from NH to SH. In this experiment, the surface information at NH is not communicated enough to the deep ocean, from there, the information could be transfered to the SH. Because of interuption of this communication forced by the fixed deep water temperature, the SH ocean and NH ocean are more like one-hemisphere ocean, but shouldered together. The downwelling portion at the NH western boundary disappeared (picture not shown). Again this demonstrates that the deep anomaly at NH is very important to set up the abyssal circulation and is the primary factor accounting for the 3-D GCM results.

4.5 Summary and discussion

In this chapter, we expanded the results of 1-hemisphere ocean to 2-hemisphere ocean. The dynamics near equatorial region is added. The underlying governing equations are very similar to those in 1-hemisphere. A 2-hemisphere, 1-basin model is developed to investigate the dynamics of the equatorially asymmetric thermohaline circulation. The model is driven only by the asymmetric surface forcing. Scaling analysis shows that the western boundary density is almost equivalent to eastern boundary density

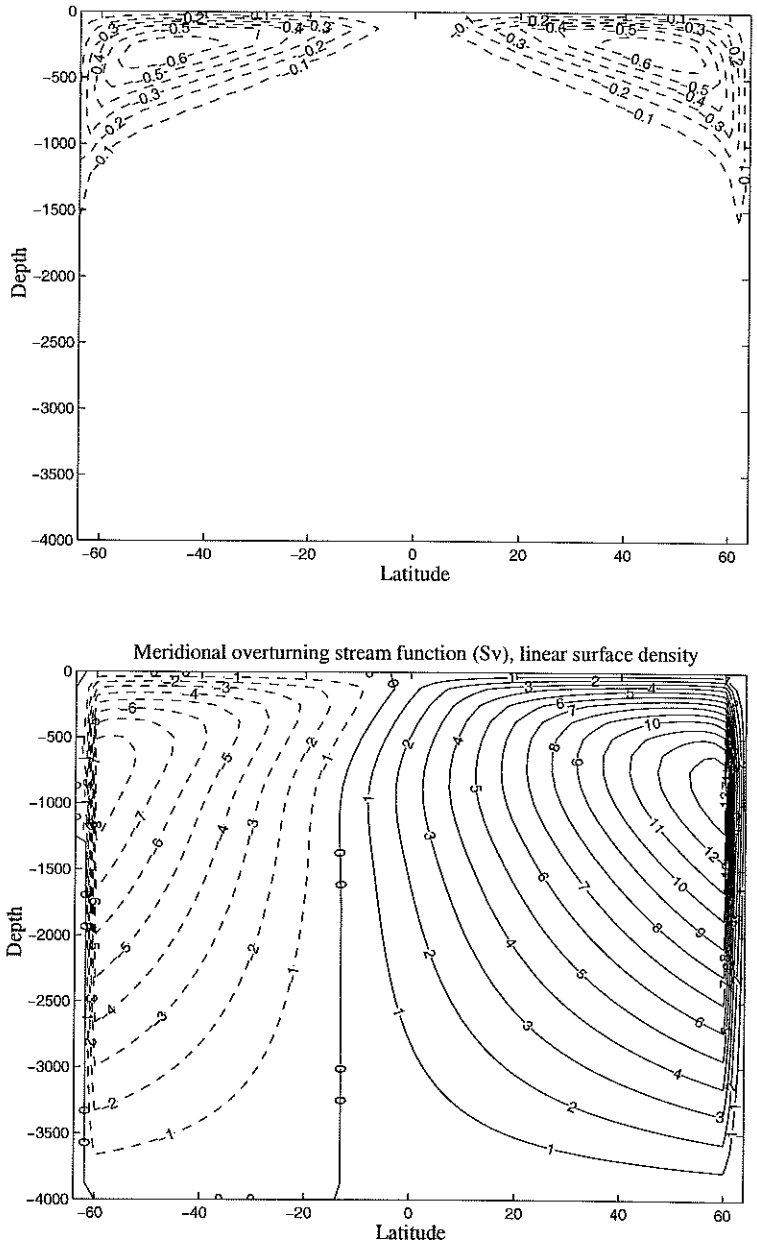

Figure 4.10: (a) Density difference as eastern wall minus western wall. Solid line: positive, contour interval $0.005 kgm^{-3}$; dash line: negative value, contour interval $0.1 kgm^{-3}$. (b) Meridional streamfunction, the flow field is clockwise around the positive value, anticlockwise around the negative value. Contour interval 1 SV.

right at the equator, therefore it is not required to impose assumption *iii*) in Chapter 2. Scaling results prove self-consistency of our model.

Our results resemble OGCM results from MK00. Especially, this model captures the main feature of their results. Namely, the equatorially asymmetric overtuning circulation, the density difference between western boundary and eastern boundary, the vertical velocity at the western boundary. In a system maintained by surface boundary conditions, a possible candidate of equatorially asymmetric circulation is the different surface density near the polar region at both hemisphere. Northern hemisphere, which in our experiment is the dominant hemisphere, contains the densest surface water, which then forms the deep water for entire abyssal circulation. It has the strongest meridional circulation. The other, subordinated SH is marked by slower circulation.

The cross-equator transport of the deep western boundary current (DWBC) demands that there is a reversal near the equator in the deep pressure (more specifically density) difference between eastern and western boundaries, due to large-scale geostrophy balance. The mechanism is analyzed from spin-up experiments (Kawase 1987, MK00). The coldest surface water at NH sets up upwelling and cold anomaly at the western boundary. This anomaly is then transfered southward, either by the mean flow, or by Kelvin waves. When it reaches equator, the dense anomaly propogates eastward along the equator until the eastern boundary is reached. Then the anomaly splits and move both northward and southward along eastern boundary. This kind of spin-up pattern is the 'seed' for equilibrium solution. This is verified in our sensitivity study when the deep water temperature is fixed, the deep density anomaly doesn't exist any longer. Cold deep anomaly is a crucial process to understand the global circulation. During the spin-up, the SH western boundary is isolated from the cold anomaly and will stay warm. It appears that the downwelling at the SH western boundary is the buoyancy source to keep warm anomalies at SH western boundary.

Unfortunately, this model could not confirm the theory proposed by MK00. One fundamental assumption of MK00 theory is that the DWBC from NH feeds entire eastern wall upwelling in the SH (Fig. 5 in MK00). The results we obtained are not very consistent with OGCM. The eastern wall upwell in the SH is much stronger, indicating that the SH western boundary perhaps is another source for SH eastern upwelling. Our simple dynamical model doesn't include the meridional velocity in the interior. This may account for the difference.

The model developed here is rather idealized and simple, though it does capture such features as the north-south asymmetry in polar density, the concomitant dominance of one hemisphere over the other in deep-water production, the upwelling over downwelling pattern of western vertical velocity in SH, the general vertical velocities in the NH. The usefulness of such an idealization of boundary-mixing model lies partly in the fact that spin-up process happens at boundaries, which serves for a rough prediction for the eqilibrium state solution. The results from this simple model also shows that the qualitative behavior illustrated by $2\frac{1}{2}$ dimensional models holds for three-dimensional dynamics. An obvious next step is to include horizontal advection terms (zonal and meridional, the latter appears more important) into our vertical advection-diffusion balance equation. The computation procedure in section 1 doesn't couple horizontal advection into density. As we know that the mean DWBC is very important to advect density southward, which then forms the deep water for the ENTIRE system. This is one of important dynamics missing from our model.

Chapter 5

Conclusion and discussion

Important issues of past, present and future climates can only be addressed if one understands the mixing process. The recent observation studies suggest that the elevated mixing near the ocean margins accounted for the 'missing mixing source' in the ocean. Boundary mixing is the key to solve the discrepancy between diapycnal mixing rates inferred from large scale budgets (Munk 1966, Hogg 1987) and those pelagic mixing inferred from turbulent micro-structure measurement.

Marotzke's (1997) numerical solution is the first attempt to explore ocean circulation models governed by mixing confined to narrow regions rather than the spread uniformly over the interior. The work of this thesis is intent to contrive a simple dynamical model representing the enhanced boundary mixing only. It was hoped that this model would mimic the results of OGCM in M97 and indeed it partially accomplished our goal. The model is then used to explore the consequences of the boundary mixing, first in 1-hemisphere, 1-basin ocean system; Secondly in global 2-hemisphere, 1-basin ocean.

The present model has the following assumptions in 1-hemisphere, 1-basin ocean.

i) Surface density is given and is a linear function of latitude; the abyss uniformly has the properties of the densest surface water.

ii) Density in the grid cells at the lateral boundary (only!) is governed by vertical advective-diffusive balance.

iii) Along the equator, isopycnals are level between western and eastern boundary.

iv) Isopycnals are flat in the zonal direction except in the western boundary current.

v) Thermal wind relation.

vi) Mass conservation.

In one-hemisphere, the thermocline scale height, D, is determined by postulating that upwelling occurs evenly over the eastern and western boundary regions and is balanced by vertical diffusion. One obtains for D and maximum overturning stream function, ψ, the expressions

$$D \sim \left[\frac{\beta y \rho_0 \Delta x}{g} \frac{L_y}{\rho_E - \rho_W}\right]^{1/3} (2K_v)^{1/3} \tag{5.1}$$

and

$$\psi = -\int W dx dy \sim \Delta x L_y (W_E + W_W) \sim \left[\frac{g}{f\rho_0}(\rho_E - \rho_W)(2\Delta x L_y K_v)^2\right]^{1/3} \tag{5.2}$$

With the surface forcing used in the numerical experiments in Chapter 2, the expression (5.2) gives a maximum overturning of 14 Sv, in good agreement of numerical result 12 Sv. The overturning streamfunction is intimately related to east and

west density difference by thermal wind balance. Only the product $K_v \Delta x$ appears in the equation. It can be interpreted as a surrogate for a small number of concentrated source regions which determines the total meridional strength.

The most pronounced evidence of the ocean circulation is the buoyancy forced upwelling and downwelling are concentrated near both lateral boundaries (Spall 2000), either using averaged uniformly mixing, or enhanced mixing over the boundaries (M97, Samelson 1998). This model captures this main feature. The vertical velocity near the western boundary is always upward, where the vertical velocity near the eastern boundary is downward over upward motion. Our model assumes that the vertical motion in both boundaries is caused by the elevated vertical mixing. Thus our model provides a dynamical link between the narrow regions which most of the meridional overturning circulation passes vertically and the large-scale, nearly zonal motions that connects these upwelling and downwelling regions. The very simple approach adopted here, mainly the mixing only exists near both lateral boundaries, allows one to infer many general consequences of boundary mixing and illuminates the fundamental role that the lateral boundaries and mixing plays in closing the three-dimensional circulation. especially

In 2-hemisphere, 1-basin ocean, the assumptions of the present model are modified:

i) The densities at north and south polar regions are different. Surface density is given and is a linear function of latitude; there is non-heat flux in the abyss.

iii) Along the equator, Rayleigh friction terms are include to overcome the singularity of Coriolis terms.

By serendipity, both propagation of Kelvin wave and DWBC are along the lateral boundaries. These dynamics are essential for spin-up process from which the equilibrium solution is predicted. The information is transfered from the surface at

dominant hemisphere to the deep ocean at the western boundary, eventually reaches the subordinated hemisphere and fills up the entire deep ocean. The asymmetry of meridional overturning is prominent even due to a small perturbation at the surface. The unidirectional DWBC is also captured by our model, which can be explained by the sign changing of the density difference between eastern and western boundaries. The density difference is always negative in the NH. Whereas in SH, it is still negative above the thermocline, but positive below the thermocline.

The model results qualitative agree with OGCM in two-hemisphere. But it is not as successful as in 1-hemisphere. The horizontal motion which links the vertical motions near boundaries and the interior, is purely zonal in our model. This could be a very unrealistic assumption, in the SH, where the horizontal circulation is very important to return water back into western boundary instead all upwell at the eastern boundary. Secondly, the meridional advection of density is central to advect cold anomaly across the equator and fills the whole abyssal ocean with these cold water. It accounts for the difference of the our overturning circulation with that of OGCM. This stresses the intent of this thesis, is to design a simple dynamical model serving as tool to understand the complex OGCM results, but not to replace the OGCM.

Appendix: Finite difference equations

Computational domain in this model is as follows: y is from 1 to 64°, and z is from 0 to -4000 m. The grid points used are 33 × 33. All the numerical values are chosen at the grid points. In the following finite difference equations, i represents y direction, y increases with latitude; j represents z direction, z increases upward.

Finite difference scheme for Eqn (2.16, 2.17) is,

$$\begin{aligned} & \frac{W_{Wi,j+1} - 2W_{Wi,j} + W_{Wi,j-1}}{(\Delta z)^2} \\ = & -\frac{g}{\beta y_i \rho_0 \Delta x}\left(\frac{\rho_{Ei,j} - \rho_{Wi,j}}{y_i} + \frac{\rho_{wi+1,j} - \rho_{wi,j}}{\Delta y}\right) \end{aligned} \tag{5.3}$$

$$\frac{W_{Ei,j+1} - 2W_{Ei,j} + W_{Ei,j-1}}{(\Delta z)^2} = \frac{g}{\beta y_i \rho_0 \Delta x}\frac{\rho_{Ei,j} - \rho_{Ei-1,j}}{\Delta y} \tag{5.4}$$

We emphasize the different numerical scheme of spatial differencing at two sides. Forward finite difference in y direction is used at western boundary, backward finite difference is used at eastern boundary. This coincides with the propagation of Kevin waves. It demonstrates how the information is transfered.

Numerical method for Eqn (2.18) is a two step predictor-corrector scheme,

$$\overline{\rho_{Wi,j}^{n+1}} = \rho_{Wi,j}^{n} - \frac{\Delta t}{\Delta z} W_{Wi,j}\left(\rho_{Wi,j+1}^{n} - \rho_{Wi,j}^{n}\right) + \gamma\left(\rho_{Wi,j+1}^{n} - 2\rho_{Wi,j}^{n} + \rho_{Wi,j-1}^{n}\right) \tag{5.5}$$

$$\rho W_{i,j}^{n+1} = \frac{1}{2}\left[\rho W_{i,j}^{n} + \rho W_{i,j}^{\overline{n+1}} - \frac{\Delta t}{\Delta z} W_{W\,i,j}\left(\rho W_{i,j}^{\overline{n+1}} - \rho W_{i,j-1}^{\overline{n+1}}\right) + \gamma\left(\rho W_{i,j+1}^{\overline{n+1}} - 2\rho W_{i,j}^{\overline{n+1}} + \rho W_{i,j-1}^{\overline{n+1}}\right)\right] \tag{5.6}$$

where $\gamma = K_v \frac{\Delta t}{(\Delta z)^2}$

The finite difference scheme for Eqn (2.19) is the same as above.

Given any initial condition of ρ_W and ρ_E, we can get W_W and W_E from Eqn (2.16) (2.17). Using Eqn(2.18) (2.19), the next step ρ_W and ρ_E are obtained. Then iteration is continued until $\|\psi^{n+1} - \psi^n\| < \epsilon$.

Bibliography

[1] Broecker, W.S., T.P. Peng, J.Houzel, and G.Russell, 1990: The magnitude of global freshwater transports of importance to ocean circulation. *Climate Dyn.*, 4, 73-79.

[2] Bryan, F., 1987: Parameter sensitivity of primitive equation ocean general circulation models. *J. Phys. Oceanogr.*, 17, 970-985.

[3] Colin de Verdiere, A., 1988: Buoyancy driven planetary flows. *J. Mar. Res.*, 46, 215-265.

[4] Ganachaud, A., 1999: Ph.D. thesis.

[5] Gargett, A.E., and G.Holloway, 1992: Sensitivity of the GFDL ocean general circulation model to different diffusivities for heat and salt. *J. Phys. Oceanogr.*, 22, 1158-1177.

[6] Gill, A.E., 1982: *Atmosphere-ocean dynamics.*

[7] Gill, A.E., and K.Bryan, 1971: Effects of geometry on the circulation of a three-dimensional southern-hemisphere ocean model. *Deep-sea Res.*, 18, 685-721.

[8] Gordon, A.L., 1986: Interocean exchange of thermocline water. *J. Geophys. Res.*, 91, 5037-5046.

[9] Gregg, M., 1987: Diapycnal mixing in the thermocline: A review. *J. Geophys. Res.*, 92, 5249-5286.

[10] Hogg, N., 1987: A least-squares fit of the advective-diffusive equations to Levitus Atlas data. *J. Mar. Res.*, 45, 347-375.

[11] Huang, R.X., and J.Yang, 1996: Deep-water upwelling in the frictional western boundary layer. *J. Phys. Oceanogr.*, 26, 2243-2250.

[12] Huang, R.X., 1999: Mixing and energetics of the oceanic thermohaline circulation. *J. Phys. Oceanogr.*, 29, 727-746.

[13] Hughes, T.C.M., and A.J.Weaver 1994: Multiple equilibrium of an asymmetric two-basin model. *J. Phys. Oceanogr.*, 24, 619-637.

[14] Kawase, M., 1987: Establishment of deep ocean circulation driven by deep-water production. *J. Phys. Oceanogr.*, 17, 2294-2317.

[15] Klinger, B.A, and J.Marotzke, 1999: Behavior of double-hemisphere thermohaline flows in a single basin. *J. Phys. Oceanogr.*, 29, 382-399.

[16] Killworth, P.D, 1985: A two-level wind and buoyancy driven thermocline model. *J. Phys. Oceanogr.*, 15, 1414-1432.

[17] Ledwell, J.R., and B.M.Hickey, 1995: Evidence for enhanced boundary mixing in the Santa Monica Basin. *J. Geophys. Res.*, 100, 20 665-20 679.

[18] Ledwell, J.R., and A.Bratkovich, 1995: A tracer study of mixing in the Santa Cruz Basin. *J. Geophys. Res.*, 100, 20 681-20 704.

[19] Macdonald, A.M., and C.Wunsch, 1996: An estimate of global ocean circulation and heat fluxes. *Nature*, 382, 436-439.

[20] Marotzke, J., P.Welander, and J.Willebrand, 1988: Instability and multiple steady states in a meridional-plane model of the thermohaline circulation. *Tellus*, 42A, 162-172.

[21] Marotzke, J., 1997: Boundary mixing and the dynamics of three-dimensional thermohaline circulations. *J. Phys. Oceanogr.*, 27, 1713-1728.

[22] Marotzke, J., and J.Scott, 1999: Convective mixing and the thermohaline circulation. *J. Phys. Oceanogr.*, 29, 2962-2970.

[23] Marotzke, J., and J.Willebrand, 1991: Multiple equilibria of the global thermohaline circulation. *J. Phys. Oceanogr.*, 21, 1372-1385.

[24] Marotzke, J., and B.A.Klinger, 2000: The dynamics of equatorially asymmetric thermohaline circulations. *J. Phys. Oceanogr.*, in press.

[25] Marotzke, J., 1999: Abrupt climate change and the thermohaline circulation: mechanisms and predictability. *The proceedings of the national academy of science.*

[26] Munk, W., 1966: Abyssal Recipes. *Deep-Sea Res.*, 13, 707-730.

[27] Munk, W., and C.Wunsch, 1998: Abyssal Recipes II: energetics of tidal and wind mixing.*Deep-Sea Res.*, 45, 1977-2010.

[28] Park, Y.G., and K.Bryan, 2000: Comparison of thermally driven circulations from a depth-coordinate model and an isopycnal-layer model: Part I. A scaling-law sensitivity to vertical diffusivity. *J. Phys. Oceanogr.*, 30, 590-605.

[29] Polzin, K.L., J.M.Toole, J.R.Ledwell, and R.W.Schmitt, 1997: Spatial variability of turbulent mixing in the abyssal ocean. *Science*, 276, 93-96.

[30] Rahmstorf, S., 1996: On the freshwater forcing and transport of the Atlantic thermohaline circulation. *Climate Dyn.*, 12, 799-781.

[31] Rooth, C., 1982: Hydrology and ocean circulation. *Progress in Oceanography.*, Vol.11, Pergamon, 131-149.

[32] Rossby, T., 1998: Numerical experiments with a fluid heated non-uniformly from below. *Tellus*, 50A, 242-257.

[33] Samelson, R.M., 1998: Large-scale circulation with locally enhanced vertical mixing. *J. Phys. Oceanogr.*, 28, 712-726.

[34] Scott, J.R., J.Marotzke, and P.H.Stone, 1999: Interhemispheric thermohaline circulation in a coupled box model. *J. Phys. Oceanogr.*, 29, 351-365.

[35] Scott, J.R., J.Marotzke, 1999: Diapycnal stirring and the meridional overturning circulation: Does it matter where the mixing occurs? Submitted to *J. Phys. Oceanogr.*

[36] Spall, M., 2000: Large-scale circulation forced by mixing near boundaries. Submitted to *J. Phys. Oceanogr.*

[37] Stommel, H., 1961: Thermohaline convection with two stable regimes of flow. *Tellus*, 13, 224-230.

[38] Toggweiler, J.R., and B.Samuels, 1995: Effect of Drake Passage on the global thermohaline circulation. *Deep-sea res.*, 42, 477-500.

[39] Toggweiler, J.R., and B.Samuels, 1998: On the ocean's large-scale circulation near the limit of no vertical mixing. *J. Phys. Oceanogr.*, 28, 1832-1852.

[40] Tziperman, E., 1997: Inherently unstable climate behavior due to weak thermohaline ocean circulation. *Nature*, 386, 592-595.

[41] Vallis, G.K., 1999: Large-scale circulation and production of stratification: effects of wind, geometry and diffusion. Submitted to *J. Phys. Oceanogr.*

[42] Warren, B.A., 1993: Why is no deep water formed in the North Pacific? *J. Mar. Res.*, 41, 327-347.

[43] Wang, X., P.H.Stone, and J.Marotzke, 1999a: Global thermohaline circulation. Part I: Sensitivity to atmospheric moisture transports. *J. Climate.*, 12, 71-82.

[44] Winton, M., 1995: Why is the deep sinking narrow? *J. Phys. Oceanogr.*, 25, 997-1005.

[45] Wunsch, C., 1970: On oceanic boundary mixing. *Deep-Sea Res.*, 17, 293-301.

[46] Wunsch, C., 1998: The work done by the wind on the ocean circulation. *J. Phys. Oceanogr.*, 28, 2331-2339.

[47] Zhang, J., R.W.Schmitt, and R.X.Huang, 1999: The relative influence of diapycnal mixing and hydrologic forcing on the stability of the thermohaline circulation. *J. Phys. Oceanogr.*, 29, 1096-1108.